

Optimal Blind Data and Channel Estimation

With Diversity

by

David P. Williams

BSc hons, University of Bath U.K., 1983

A Thesis Submitted in Partial Fulfillment of the Requirements for the Degree of

Master of Science in Engineering

in the Graduate Academic Unit of Electrical and Computer Engineering.

Supervisor: Professor Brent R. Petersen, Electrical and Computer Engineering

Examining Board: Professor James H. Taylor, Chair, Electrical and Computer Engineering

Professor Rodney H. Cooper, Computer Science

Professor Rajamani Doraiswami, Electrical and Computer Engineering

Professor Richard J. Tervo, Electrical and Computer Engineering

This thesis is accepted

Dean of Graduate Studies

THE UNIVERSITY OF NEW BRUNSWICK

April, 2003

© David P. Williams, 2003

Dedication

This thesis is dedicated to my wife and family.

Abstract

For a single user scheme with frequency dependant channel, a generalized maximum likelihood sequence estimation (MLSE) algorithm was demonstrated to improve the performance over the single antenna method. It achieved almost perfect combining using blind joint data and channel estimation by means of combining of metrics from two antenna diversity. The dominant cause of errors was due to the presence of two trellises with almost identical metrics and these trellises were related being the same sequence delayed by plus or minus one sample period. This was especially prone to happen when the estimated model order was not the true order. Another difficulty with this algorithm was the reduction in the number of choices for trellises entering a state as the trellises tended to converge to the best one; this provided a larger exhaustive search at the beginning of the algorithm than later when fading affected the channel.

Acknowledgements

I wish to express my sincere gratitude to my research advisor Dr. Brent R. Petersen for his continued support and guidance during this project. I have made numerous mistakes and have found him understanding and tolerant. It has been a rewarding experience working with him. To fund a literature search he was able to use an Operating Grant that was provided by the Natural Sciences and Engineering Research Council (NSERC).

I am also grateful to my wife and family for their support during the process.

Table of Contents

Dedication	ii
Abstract	iii
Acknowledgements	iv
Table of Contents	v
List of Tables	viii
List of Figures	ix
List of Symbols	xi
Abbreviations	xiii
Chapter 1 Introduction	1
1.1 Motivation	1
1.2 Goal of this thesis.....	2
1.3 Discussion of previous work and references.....	3
Chapter 2 System Description.....	11
2.1 Diagram and explanation.....	11
2.1.1 Signal to noise definition	13
2.1.2 1xEVDO information used.....	15
2.1.3 Application of the generalized VA by Seshadri to include diversity..	16
2.1.4 Steps in the simulation sequence	21
2.2 Incorporation of diversity.....	26
2.2.1 Derivation of metric calculation.....	26
2.2.2 Different orders for each path	29

Chapter 3 Results of Computer Simulation of Single User Scheme.....	31
3.1 Selection of channel impulse responses used for simulation.....	31
3.2 Consequences of the optimal combining of a second antenna.....	34
3.3 Effect of model order mismatch, between the true and estimated model. ...	39
3.4 Convergence of M trellises per state.....	44
3.5 Consideration of “slippage”.....	50
3.6 Comments on assumptions and sources of error.....	62
Chapter 4 Conclusions and Future Improvements.....	65
4.1 Performance	65
4.1.1 Improvement by the optimal combining of a second antenna.	65
4.1.2 Operation during start up.	66
4.1.3 Performance after convergence of M trellises.	67
4.2 Suggestions for Future Improvements	67
4.2.1 Control order of CIR estimate to avoid “slippage”	67
4.2.2 Multi-user version for CDMA use	68
References.....	69
Appendixes.....	72
A. Transmit and receive filter frequency response	72
B. Algorithm performance with reference CIR	74
C. More results.....	76
D. Number of complex calculations per sample	80
E. Eye diagram.....	82
F. Zeros of the CIRs used.....	83

G. Learning CIRs for multiple users 84

List of Tables

2.1.2-1	1xEVDO characteristics used in numerical simulations.....	15
2.1.4.1	The values used for the experiment in Section 3.2.....	21
3.1-1	Coefficients of the CIRs used for performance simulations.....	31
3.3-1	Mean errors for various estimated CIR orders using CIR2.....	42
3.3-2	Mean errors for various estimated CIR orders using CIR1.....	43
3.3-3	Mean errors for various estimated CIR orders using CIR3.....	43
3.3-4	Mean errors for various estimated CIR orders using CIR4.....	43
D-1	Number of complex calculations required per sample.....	80
D-2	Example of number of complex calculations.....	80

List of Figures

2.1-1	Diagram of complex baseband model.....	11
2.1.1-1	Illustration of S/N definition.....	13
2.1.3-1	DSA flow diagram for two antenna diversity.....	18
2.2.2-1	Illustration of how to deal with CIRs of different orders.....	29
3.1-1	Channel impulse responses used for computer simulation.....	32
3.1-2	Frequency responses of CIRs used.....	32
3.1-3	Eigenvalue spread of the CIRs used in the simulations.....	33
3.2-1	Improvement of BER performance by optimal diversity combining.....	35
3.2-2	Start up performance with diversity.....	36
3.2-3	Distribution of errors over length of trial.....	38
3.3-1	Performance of mismatched orders when the true order was five..	39
3.3-2	Performance with different true CIR orders.....	41
3.4-1	Convergence of all M trellises kept per state to the same trellis....	47
3.4-2	Comparing diversity to computing M trellises.....	49
3.5-1	Illustration showing slippage in the CIR estimate.....	51
3.5-2	Example of the distribution of number of errors in 20 trials.....	52
3.5-3	Evolution of expected value of error for two CIRs showing difference between no slip and slip of one sample delay.....	57
3.5-4	Final mean squared error from LMS algorithm with two CIRs using data with no slip and slip of one sample delay.....	58
3.5-5	Accumulated metric from one trial showing two slippages at the start up and later in the trial.....	59
3.5-6	CIRs without first and last coefficients equal.....	61

A-1	Transmit and receive filter coefficients and frequency response...	72
B-1	Results for reference CIR = 1, using single and diversity antennas.....	74
B-2	Corrected reference BER performance for reference CIR.....	75
C-1	Variation of trellis length.....	76
C-2	Variation of μ in LMS algorithm for CIR updating for two antenna diversity.....	77
C-3	Performance with start up errors removed.....	79
E-1	Eye diagram for CIR2, 15 dB S/N ratio and 25 % excess bandwidth.....	82
F-1	Zeros of CIRs used showing which have non-minimum phase.....	83
G-1	Resulting CIR estimates for 3 active user codes and 47 unused codes.....	84

List of Symbols

A	Number of antennas used
C	Channel impulse response including transmit and receive filters.
$\hat{C}R$	Estimated CIR
d	Data
d_{in}	Differential data from TX
d_{out}	Differential data detected from algorithm
E	Expectation operator
ε	Noise signal at output of filter
e_0	Error of estimated sample.
$F(.)$	Discrete Fourier transform realized by the fast Fourier transform
$F^{-1}(.)$	Inverse Fourier transform.
f	Frequency
g	Zero memory non-linearity function
H	Filter frequency response
J	Metric
J_{min}	Minimum mean squared error.
$J_{ex}(\infty)$	Excess mean square error due to LMS.
K	Weight-error correlation matrix
k	Index to states in trellis matrix
k	Index shift for correlation
L	Length of true CIR
M	Number of trellises kept per state
m	Signal at output of the CIR
N	Length of trellis
n	Index to samples processed.
η	Noise
O	Order of estimated CIR

P	Probability density function
p	Cross-correlation of desired signal and received signal
Q	Number of signalling levels
R	Correlation matrix of received samples
$\Re(.)$	Operator for finding the real part of (.).
r	Received signal
\hat{r}	Estimated received signal
S	Candidate sequence or trellis
T_s	Symbol period
$Toeplitz(.)$	Operator for generating a Toeplitz matrix from the vector (.)
T_x	Transmitted data sequence
U	Number of possible user codes
v	Number of samples within the CIR when over sampled
w	Number of samples left after v were split from all the samples
y	Equalizer output
Z	Matrix of the over-sampled CIR
α	Filter roll off factor
δ	Slip delay
μ	LMS step size
λ	Eigenvalue
\aleph	Number of samples in a trial.
σ^2	Noise variance
σ_d^2	Variance of the desired signal

Abbreviations

ALC	Automatic level control.
BER	Bit error rate.
BPSK	Binary phase shift keying.
CDMA	Code division multiple access.
CIR	Channel impulse response.
MCIR	Mis-adjustment of CIR.
dB	deciBel.
DFSE	Decision feedback sequence estimation.
DSA	Diversity with Seshadri's algorithm
EXBW	Excess bandwidth.
FIR	Finite impulse response.
ISI	Inter symbol interference.
LMS	Least mean square.
MLSE	Maximum likelihood sequence estimation.
<i>MSE</i>	Mean squared error.
NSERC	Natural Sciences and Engineering Research Council
PN	Pseudo noise.
PSP	Per-survivor processing.
RLS	Recursive least squares.
RSSE	Reduced state sequence estimation.
RX	Receiver.
S/N	Signal to noise ratio.
TX	Transmitter.
VA	Viterbi algorithm.
1xEVDO	First evolution data only.

Chapter 1 Introduction

1.1 Motivation.

In many digital communication applications wireless is preferred as shown by the success of the cellular telephone, which allows the users to be mobile. The wireless environment is complicated by the effect of multi-path on the received signal and the cellular environment is characterized by interference caused by all the other users. Multi-path effects are frequency selective fading that cause inter-symbol interference (ISI) or complete loss of the signal. Movement by the users and of the objects reflecting the signal to the receiver causes the path to change.

Outside of the communications field geo-science and image restoration could also be targets for this blind data and channel estimation technique.

To counteract these effects the multi-path can be estimated and MLSE used. Some of the recently developed detectors are described as blind. They do not need a training sequence from the transmitter (TX), which means the receiver (RX) can adjust itself, without interrupting the transmission of data to other users, without waiting for the next training sequence or when the signal has been recovered after fading.

By generating specific results with some numerical simulations the effectiveness of this joint blind data and channel estimation with diversity technique was demonstrated. Elements of the simulations in this thesis were based on the commercial standard 1xEVDO. 1xEVDO, also known as High Data Rate, or IS-856. This was chosen by the designers because it was a high-performance and cost-effective Internet solution.

For the user of this technique the advantages enjoyed would include these. At the transmitter there would be no need for the training sequence or preamble to be transmitted. This would allow a higher user data transfer rate by reducing overhead and longer battery life by reducing the time taken to transmit the data. The receiver may also recover after a deep fade during a frame, rather than wait for the next training sequence.

These advantages come at a price; there would be a great increase in processing and for diversity an extra antenna with filtering, frequency conversion and sampling would be required. Even so errors can still be caused by a problem called slippage. Slippage was discussed in this thesis as a problem which limited the performance of the technique. Slippage was likely to occur and caused frequent errors in the received data output if the estimated channel impulse response (CIR) order was not the true one or the true CIR had small magnitudes at its beginning or end.

1.2 Goal of this thesis.

The new contribution described in this thesis was the demonstration of the effective use of diversity with joint blind data and channel estimation, by extending Seshadri's [Ses94] work to diversity with Seshadri's algorithm (DSA), using the combination of two inputs in an optimal manner to considerably reduce bit error rate. Some difficulties were also pointed out.

In Section 2.2 the background to the combination of two inputs with the use of the sum of the squared errors was developed to drive a type of generalized Viterbi algorithm (VA). This hypothesis was tested in some experiments by the use of numerical simulation, described in Section 2.1.4. The results for the non-fading multi-path CIRs for a single user scheme were shown in Chapter Three. Since a blind receiver would not

know the true CIR order, lower and higher estimated CIR orders were compared to the real path order for bit error rate (BER) performance in Section 3.3. Observations about the resulting performance in terms of BER were synthesized into a conclusion in Chapter 4.

1.3 Discussion of previous work and references.

The digitally implemented adaptive equalizer concept was introduced by Lucky of Bell Laboratories [Luc66], and has been extended over the last 36 years to include a multitude of algorithms. These were useful for high data rate mobile communication systems. Proakis [PrNi91] defined blind reception as a signal processing technique that recovers the input sequence applied to a linear time-invariant non-minimum phase channel from its output only. The algorithms were essentially adaptive filtering algorithms designed in such a way that they did not need the external supply of a desired response to generate the error signal.

According to Chen and Hoeher [ChHo01] there were three categories of these blind reception techniques, first those based on statistical properties of the received signal, second those that exploited the algebraic structure of over-sampled systems called the deterministic or sub-space approach, and third those that used trellis-based techniques.

Examining the first category, these were techniques based on the statistical properties of the received signal. Sato was the first to publish a paper on blind equalization [Sat75]. The most widely used algorithm was attributed to Godard [God80], sometimes called the constant modulus algorithm. These were based on the steepest descent and being basically a least mean square (LMS) type of algorithm they were

limited by their relatively slow convergence and potential to converge to a local minimum with poor performance. Both the Sato and Godard algorithms could be regarded as special cases of the Bussgang algorithm as formulated by Bellini [Bel86]. The Bussgang algorithm applied a memoryless nonlinearity, that was a kind of slicer, at the output of the equalization filter in order to generate the desired response. This output took the place of the desired response for the LMS adaptation algorithm. The term Bussgang [Bus52] was used to indicate the class of stochastic processes that satisfy the condition, $E[y(n)y(n-k)] = E[y(n)g(y(n-k))]$, where y was the equalizer output, E was the expectation operator, g was the zero memory non-linearity function, n was an integer index to the samples of y and k was the index shift for correlation. That means the process had an auto-correlation function equal to the cross-correlation of the process and the output of the memory non-linearity produced with that process. This was relevant since the blind equalizer was driven by the error of the difference between the equalizer output, $y(n)$, and the output of the zero memory non-linearity, $g(y(n))$, and for the algorithm to converge the error should tend to zero so the expected values should tend to be equal.

Still within the first category, there were higher-order statistics, which were described in terms of cumulants and their Fourier transforms known as polyspectra. Polyspectra provide the basis for the identification of non-minimum phase channels because they preserved phase information from the channel output unlike the auto-correlation or power spectral density. From the estimate of the fourth-order polyspectra, called the tricepstrum, the identification of the channel could be done and then an equalizer made by inverting the channel. Hatzinakos and Nikias [HaNi91 and HaNi94]

published this algorithm. These were much more computationally intensive than the Bussgang type, but both suffered from slow rate of convergence, compared to the conventional adaptive filter with a training sequence.

In the second category another statistical property was used, its cyclostationary, which meant the auto-correlation of the received signal was periodic in the symbol duration. Tong et al. [ToXuKa91] was credited with the first application of this to blind reception. His idea was to use over-sampling of the received signal. This was also called fractionally spaced equalization, as described by Gitlin and Weinstein [GiWi81] for the non-blind case. Over-sampling may have been replaced by using multiple antennas each sampled at the symbol rate. For an example of this technique by Tong et al. [ToXuKa94] the auto correlation matrix R_x of the received signal was used to estimate the noise variance and length of the CIR. They considered a vectorized process and its correlation matrix,

$$r(n) = Zs(n) + \eta(n), \quad (1.3.1)$$

$$R_x(k) = ZR_s(k)Z^H + R_n(k), \quad (1.3.2)$$

where r was the received signal sequence, R_s was the correlation matrix of the desired signal, R_n the correlation matrix of the noise, s was the data symbol, η was the noise, Z was an $v \times w$ matrix of the over-sampled CIR where v was the number of samples within the length of the CIR and w was the number of samples left after v were taken away from the total samples used. These estimates were used to correct the estimate for noise and an estimate of Z could then be found from the singular vectors and singular values which came from the singular value decomposition of R . Once Z was found the CIR could be recovered from it and used to extract the data by equalizing or maximum likelihood techniques.

In a way this second category could be considered similar to the recursive least squares (RLS) algorithm in that it used a correlation matrix, as opposed to the LMS used in the Bussgang techniques. The major advantage over the first category was the use of second-order statistics rather than higher-order statistics, however the processing still needed to be carried out at a higher rate because samples were taken faster than the incoming symbol rate and single value decomposition of correlation matrices needed to be found. It was also necessary to find the signal to noise (S/N) ratio and channel order as well, compared to the maximum likelihood algorithm used in this thesis where it turns out that only knowledge of the channel order would be required.

An advantage of using MLSE rather than equalization was that the inverse of the CIR was not found which avoided the noise enhancement on those channels with spectral nulls.

For the third category the maximum likelihood criterion was extended, so that according to Biglieri et al. [BiPrSh98] for a Gaussian channel the joint probability density function, P , of the received data vector $r = [r_1 \ r_2 \ \dots \ r_N]^T$ for a block of N data was

$$P(r|CIR, d) = \frac{1}{(2\pi\sigma^2)^N} \exp\left(-\frac{1}{2\sigma^2} \sum_{n=1}^N \left| r_n - \sum_{k=0}^L CIR_k d_{n-k} \right|^2\right), \quad (1.3.3)$$

where d was the data vector $d = [d_1 \ d_2 \ \dots \ d_N]^T$, L was the length of the true CIR and σ^2 the noise variance. Since neither d , nor σ^2 nor CIR was known one way to maximize the probability was to determine an estimate of CIR for every possible sequence. It was possible to do because every possible sequence came from a finite alphabet with known statistics, independent and identically distributed. Then the sequence was selected that minimized

$$\sum_{n=1}^N \left| r_n - \sum_{k=0}^L CIR_k d_{n-k} \right|^2 \quad (1.3.4)$$

for each CIR, which maximized the probability, however this was an exhaustive search with computational complexity that grows exponentially with the length N . If $N = L$ there will be one CIR estimate for each surviving path of the VA search through the trellis, this was the approach of Raheli et al. [RaPoTz95] and of Chugg and Polydoros [ChPo96]. Seshadri's [Ses94] scheme was similar but used a generalized VA that retained $M \geq 1$ best estimates at each state of the trellis along with corresponding CIR estimates. Up to the first $N = O + \log_2(2M)$ stages in the trellis search were exhaustive, where O was the order of the estimated CIR, and from then on the limit M made the process practical. He showed good performance was achieved by setting M to four and this was used in this thesis for the study of performance using two antenna diversity.

Raheli et al. [RaPoTz95] proposed per-survivor processing (PSP). This technique cancels the effects of (ISI) within the calculation of the metric used in the VA, based on the data sequence that lead to the survivor. They pointed out that the technique was not confined to unknown CIR but also carrier phase or symbol timing error, and suggested that PSP was the generalized interpretation of reduced state sequence estimation (RSSE). PSP was related to RSSE and decision feedback sequence estimation (DFSE) by the use of tentative decisions when there was uncertainty in any channel parameters while RSSE and DFSE treated particular parameters, both reduced order and mis-adjustment of CIR or just reduced order CIR respectively. DFSE was described by Duel and Heegard [DuHe85]; it reduced the number of states by using a remaining ISI correction. RSSE was also described by Eyuboğlu and Qureshi [EyQu88]; it was a generalized case of

DFSE, where the reduced states were chosen by reducing the number of possible transitions from any state. This was relevant when the modulation scheme uses more than one bit per symbol. In this thesis the algorithm reduced the number of trellises to M rather than one as with RSSE. As illustrated by Seshadri and Anderson [SeAn88] the M algorithm deleted all but M states, using the lowest accumulated metric to choose them, then the trellis with the lowest accumulated metric was used to give the best estimate of transmitted symbol. They also mentioned that use of decision feedback introduces error propagation.

By making the number of states variable rather than set to M , Simmons [Sim90] called this the T-algorithm, although this would have been a possible improvement it was not included to allow comparison of the use of one antenna or two antenna diversity to be evident.

Zervas, Proakis and Eyuboğlu [ZePrEy92] had suggested a similar algorithm to Seshadri but avoided the estimation of the CIR by LMS for each state. Rather a CIR was assumed and the optimum sequence for this CIR found, then the CIR was modified and the optimization repeated using the same data sequences, this modification of the CIR improved the CIR estimation.

Since 1994 there has been some work published that references Seshadri's paper [Ses94]; these following authors were those that developed his idea. The majority that reference his work did so to illustrate the high computational load and they then went on to suggest some less intensive algorithms; see appendix D for the load of the algorithm used in this thesis.

Non-linear channels were addressed by Jeng and Yeh [JeYe97] with blind clustering for non-linear channels which would have been useful to account for those non-linearities from TX power amplifiers. Clustering was mentioned by Seshadri but in the context of finding the noise free constellation and subsequently applying his algorithm.

The technique of using a finite alphabet was combined with the second category, sub-space approach, by van der Veen, Talwar and Paulraj, [VeTaPa97]. This addresses the multi-user and multi-antenna case with an extremely complex algorithm using over sampling as the sub-space approach did. Their algorithm relied on the finite alphabet to perform the multi-user separation.

Chen and Luk [ChLu99] proposed a two-stage approach to optimizing the joint data and channel estimate, similar to the algorithm proposed by Zervas, but coefficient annealing was used to modify the CIR. Coefficient annealing was a class of guided random search by adjusting the CIR coefficients differently for the LMS or RLS algorithms.

Chen and Hoeher [ChHo01] used two different techniques compared to Seshadri, they used RLS instead of LMS to the CIR update, and coefficient annealing to avoid converging to a local minimum. They also mentioned slippage, calling it shift ambiguity and suggested the solution is to maximise the S/N ratio but this would require some further processing; see suggestions for further work Section 4.2. Another solution they provide was to rely on coefficient annealing to make the CIR move from a local minimum to the global minimum or true CIR.

Regarding the use of PSP with code division multiple access (CDMA) systems such as 1xEVDO Hong, Joo and Lee [HoJoLe01] suggested the use of the pilot available on the reverse link with these systems. This showed how multi-user separation could be achieved but did not address the use of antenna diversity; see Section 4.2 further work for suggestions on combining the two.

This thesis stayed with the least complicated algorithm to demonstrate the performance of the diversity combining technique. The ideal situation would have been to make M so large that no paths were discarded until the CIR was learnt however the attraction of Seshadri's work was to use a low value of M to make the process practical. Choosing a value of M made an ad hoc solution so some or all of the above variations could have been applied and would have improved performance at the cost of more processing.

Chapter 2 System Description

2.1 Diagram and explanation.

By defining the path CIR as a finite impulse response (FIR) filter with the number of coefficients being the order of the filter L , the following model allowed simulation by computer, which assumed a linear channel. The object of the up-sampler was to raise the sampling rate so the TX filter could be applied without aliasing the wanted signal, it was implemented as shown in Section 2.1.4.

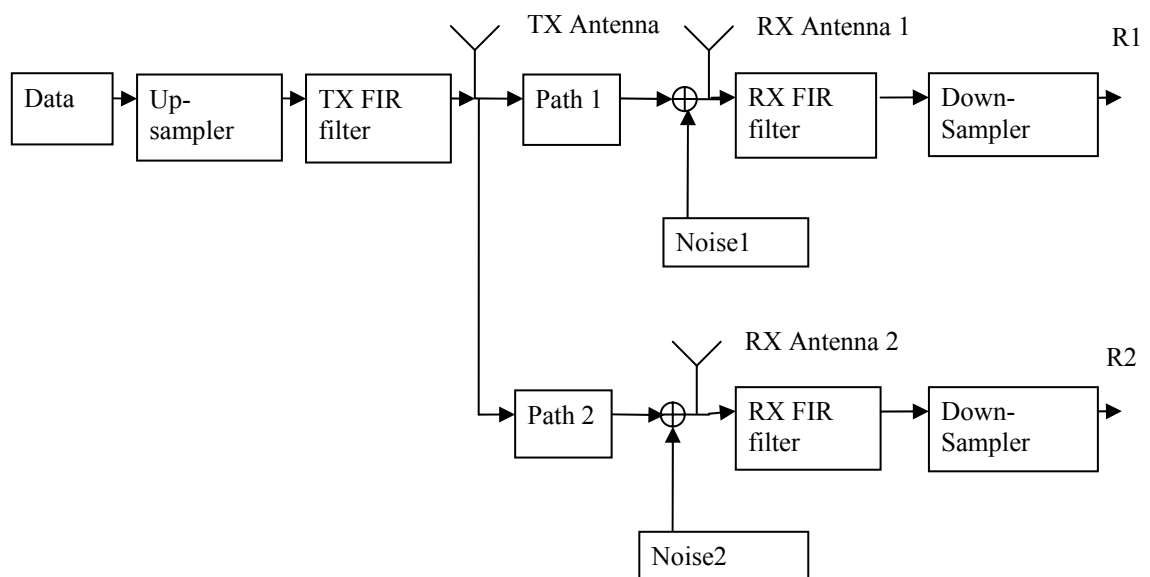


Figure 2.1-1 Diagram of complex baseband model.

For the parts of a practical RX that were not modelled the assumptions used were that synchronization of frequency, phase, and symbol have been achieved, and a level control technique was used to set the power level of the signal entering each sampler to

avoid weighting the diversity combiner. To restrict the bandwidth of the transmitted signal and to try to avoid inter-symbol interference, square root raised cosine filters were used for both the transmit and receive filters. For all the simulations an excess bandwidth of 25% was used, the number of coefficients per transmitter filter was 33, see Appendix A for more details. Samples from the down-sampler were then passed to the estimation algorithm sampled at symbol rate. Even though sampling at the symbol rate caused significant information loss as the information bandwidth is not less than half the sampling frequency, here the method used by Seshadri was followed. As Gitlin and Weinstein [GeWi81] pointed out fractionally-spaced sampling can deal with timing uncertainty and more generally can deal with delay distortion. Improved performance could be expected with fractionally-spaced sampling but in the interests of simplicity to compare single and diversity antenna algorithms it was not used.

To compare the performance of the DSA, the matched filter bound was used, forming a lower bound on the expected performance, the best possible receiver unimpaired by ISI, Wozencraft et al. [WoJa65]. The matched filter bound was obtained assuming the data symbols suffered neither ISI nor interference, only additive noise, Lucky et al. [LuSaWe68].

When the channel was invariant, discussed in Section 2.1.2, the received complex baseband signal $r(t)$ was represented by

$$m(t) = \sum_{k=-\infty}^{\infty} d_k C(t - kT), \quad (2.1.1)$$

$$r(t) = m(t) + \eta(t), \quad (2.1.2)$$

where d_k was a data symbol from the finite alphabet +1 and -1, m was the signal coming out of the CIR, C included the transmit and receive pulse shaping filters and the CIR, and T was the symbol period.

2.1.1 Signal to noise definition

The S/N was defined by measuring the average signal power at the receiver antenna in the system diagram below. From the signal power and the required S/N, the variance of the noise was adjusted to get the required average noise power.

$$\frac{S}{N} = \frac{\overline{m^2}}{\overline{\eta^2}} = \frac{\frac{1}{\aleph} \sum_{i=1}^{\aleph} m_i \times m_i^*}{\frac{1}{\aleph} \sum_{i=1}^{\aleph} \eta_i \times \eta_i^*}, \quad (2.1.1.1)$$

where η was the noise signal coming out of its TX filter, \bullet^* was the complex conjugate of \bullet , and \aleph was the number of samples.

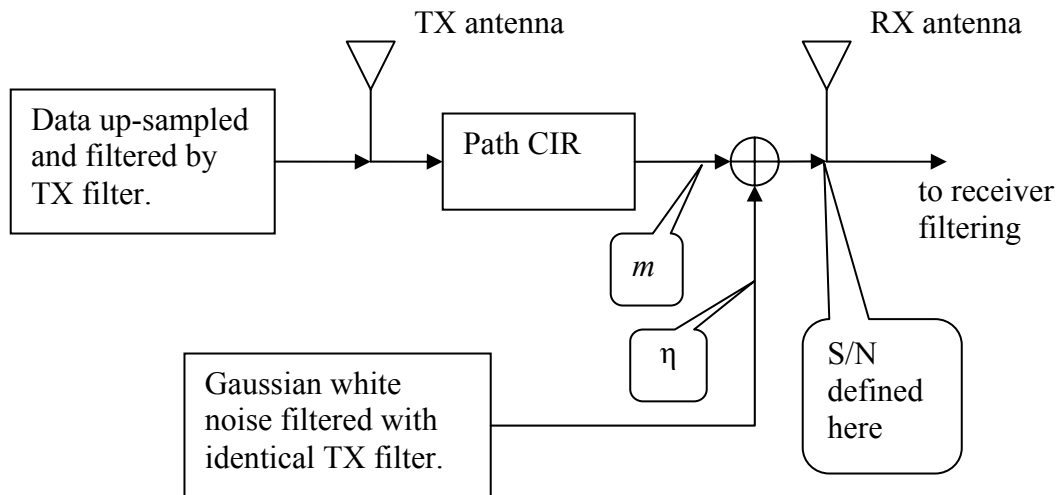


Figure 2.1.1-1 Illustration of S/N definition.

The bandwidth of the signal m was set by the transmit filter and CIR. The noise was a Gaussian wideband signal that was band-limited by an identical filter to that used in the transmitter. This choice was probably better than the real life case as the wideband noise would be filtered by the tuned circuits and filters of a real receiver which would be wider than the transmit filter until it got to the receive filter in Figure 2.1-1, however the choice of what bandwidth and roll off to use is more complicated than justified for this work and this choice reduces the number of variables to be taken into account.

In the diversity case the S/N was set equal at both RXs. The signal and noise powers were the same at each antenna. The same signals and noise were applied to the single antenna simulations and each antenna in the diversity simulation. At each antenna the noise was assumed to be independent, this was valid as long as it was assumed that there was no common dominant source of noise such as interference from outside the receiver or a common local oscillator in the receiver. There was an issue regarding the S/N definition with the diversity case as the received signals did not have a cross correlation of zero due to them being the same source passed through different filters, however using the same signals seemed to reflect the practical model of placing the antennas. In the work by Schlagenhauser et al. [ScPeSe99] the S/N was defined as the sum of the S/N at each antenna. This was not used as it would have required the S/N at the two antennas to be changed to compare the single antenna and diversity techniques at the same S/N. That would have implied a different physical configuration and raised the question of how that would be in practice. This thesis assumed the antennas were in the same position and received the same signals which were unaffected by the presence of the other antenna.

2.1.2 1xEVDO information used.

By generating specific results with some numerical simulations modelling elements of the commercial standard 1xEVDO, also known as High Data Rate, or IS-856, some idea of the performance with modern applications was gathered. The 1xEVDO standard had a pilot available in all reverse modes, the slots were synchronized and used a preamble in the reverse access mode; to look at the recovery from fading none of these was used in this thesis. The access point or base station had a pilot-aided, coherently demodulated reverse link, which was assumed for synchronization.

From the 1xEVDO specifications produced by the 3GPP2 organization in document C.S0024 [1xEVDO] the characteristics shown in Table 2.1.2-1 were used in this thesis based on the reverse channel and the highest data rate.

Characteristic	Value
Data rate	153.6 kb/s
PN chip rate	1.2288 Mchips/s
Modulation type	BPSK
Path delay spread	5.5 μ s
Coherence time	1 ms, (carrier 1.9 GHz, velocity 100 km/h)
Coherence bandwidth	36 kHz
CIR	[1 1 0 0 0 0.7]

Table 2.1.2-1 1xEVDO characteristics used in numerical simulations.

Application of the DSA was done before de-correlation of the CDMA signal in this case as de-correlation using a known spreading code removed the object of the blind scheme, because the spreading code period was longer than the CIR. This also meant that multi-user CDMA environment was not possible with this algorithm as used in the numerical simulation, so the chips were the data symbols as the multi-user coding was not required. However some results on the convergence of multiple CIR estimates are in Appendix G.

Comparing the coherence bandwidth with the PN chip rate, where PN was pseudo noise, showed that the signal would suffer some distortion in frequency response. However the coherence time and PN chip period indicated that the distortion would stay constant for approximately 1200 chips, which should allow the estimated CIR to converge, and was used as the number of samples in all the trials. If fading had been included and it was slow it was expected that the algorithm would track the true CIR.

2.1.3 Application of the generalized VA by Seshadri to include diversity.

Define the state of the trellis as the data applied to the coefficients of the CIR. Q was defined as the number of signalling levels, Q was two for BPSK. M was defined as the number of trellises kept per state. N was the total length of the trellis kept. O was the length of the estimated CIR.

From Seshadri's paper [Ses94] the optimal blind sequence estimator used every single sequence that could be transmitted, however the error metrics used depend on the estimation of the CIR which are inaccurate at the beginning so ideally no trellises should be dropped until the correct CIR has been converged to. This is the reason why the number of paths leading to each state should not be left at one as in the VA, by saving as many paths as possible for as long as possible the probability of still having the correct trellis is improved even though the CIR estimates may be inaccurate at the beginning. To keep all the trellises until the CIR had converged would have taken approximately $10L$ samples, the trellis matrix would be $10L \times Q^{11L}$, this is the classic stumbling block of this technique as the size increases rapidly with L . The novel part of Seshadri's algorithm was that each of the states had more than one surviving trellis but less than Q^{10L} ; it was reduced to manageable size by RSSE techniques. As Seshadri suggested the

M algorithm was employed where $M \leq Q^L$ and M trellises were kept for each state, along with their associated error metric and path estimate. As in the normal VA the length of the trellis was truncated at 10L to allow data to be recovered without waiting for the whole message to be received.

For each path in the trellis the algorithm estimated the next received symbol and generated the error metric. The metric was found by comparing the estimate to the actual received signal for each candidate. A metric similar to the VA was used to choose the surviving trellises. For the case of $M = 1$ the metrics J would be:

$$J_k^n = \min \left\{ \begin{array}{l} J_k^{n-1} + \left[r_1(n) - \sum_{i=1}^O \hat{C}IR1_i^k \text{state}_i \right]^2 + \left[r_2(n) - \sum_{i=1}^O \hat{C}IR2_i^k \text{state}_i \right]^2 ; \\ J_k^{n-1} + \left[r_1(n) - \sum_{i=1}^L \hat{C}IR1_i^k \text{state}_i \right]^2 + \left[r_2(n) - \sum_{i=1}^L \hat{C}IR2_i^k \text{state}_i \right]^2 \end{array} \right\}, \quad (2.1.3.1)$$

where J_k^n was the accumulated metric with diversity for state k and sample n , r_1 was the signal received from antenna 1 and r_2 was the signal received from the diversity antenna 2, $\hat{C}IR1$ was for the path to receiver 1, and $\hat{C}IR2$ was for the path to receiver 2, k was the index to the state. Extending this to $M > 1$ was achieved by choosing to 2 from 4 or 4 from 8 and so on. Then the M trellises with lowest J_k were chosen for each state, and the CIR estimate was done using the LMS algorithm as shown in Figure 2.1.3-1. Once the first 100 samples were received the differential data was detected by using the oldest two data in the trellis which had the lowest accumulated metric. Using the relatively slow, but robust, LMS algorithm was justified here as the channel was found to be slow fading compared to the high data rate.

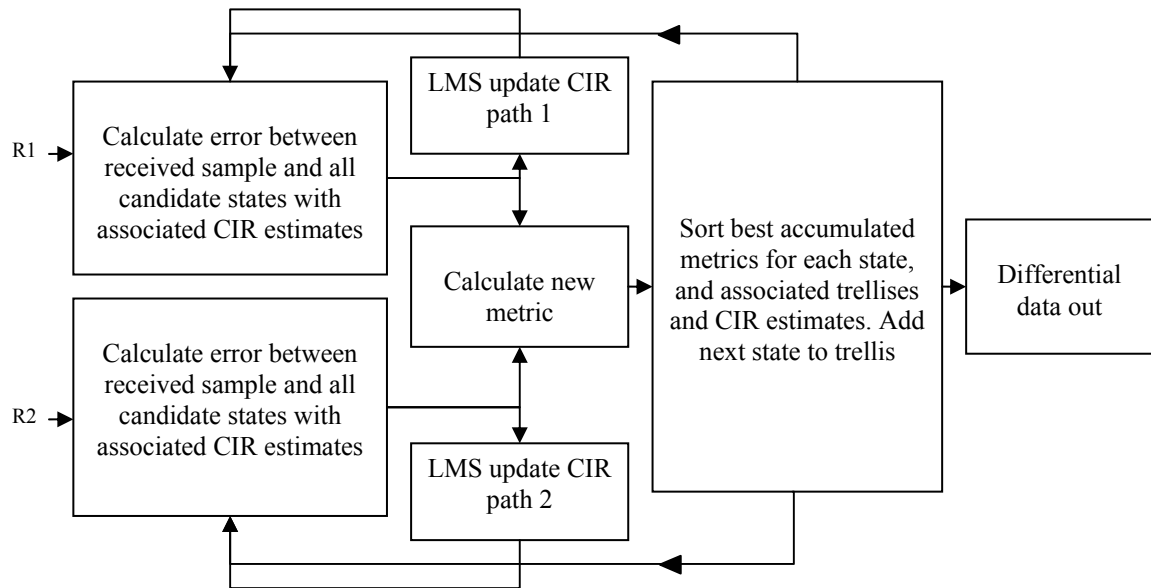


Figure 2.1.3-1 DSA flow diagram for two antenna diversity.

In all the simulations the input data distribution was assumed to be symmetric so no clue could be gained as to the sign of the transmitted sequence. Therefore there was ambiguity between the data sequence d with its CIR and the sequence $-d$ with $-CIR$, so differential coding was used to overcome this problem.

It was thought that a reduction in the number of trellises, and their associated metrics and path estimates could be done by recognizing that when a particular data sequence had been assigned as that leading to a state in the trellis its complement would automatically be assigned the complement path estimate and so the same metric, thus the complementary trellis, metric and path estimate would not have to be stored. However this was not what occurred as the algorithm ran recursively. An example using $O = 3$ showed how the complementary states were generated naturally and why they needed to be followed individually.

If 3 bits per state were used the total number of states would be $Q^3 = 8$ of which only $Q^3/2 = 4$ states were non-complementary and needed to be considered,

$$\begin{array}{ccc} +1 & +1 & +1 \\ +1 & +1 & -1 \\ +1 & -1 & +1 \\ +1 & -1 & -1 \end{array} \quad (2.1.2.1)$$

the other possible combinations are all complements of one of these rows.

The next possible states for each of those previous states are

$$\begin{array}{cccccc} +1 & +1 & +1 & +1 & +1 & +1 \\ +1 & +1 & -1 & +1 & -1 & +1 \\ +1 & -1 & +1 & -1 & +1 & +1 \\ +1 & -1 & -1 & -1 & -1 & +1 \end{array}, \begin{array}{ccc} +1 & +1 & -1 \\ +1 & -1 & -1 \\ -1 & +1 & -1 \\ -1 & -1 & -1 \end{array} \quad (2.1.2.2) \text{ each}$$

of the previous states had it's corresponding path estimate and sequence of data and metrics leading up to it, and those should be passed along with the surviving trellises but looking at the lower two rows these have next states which did not form part of the set being used. The swapping with the complementary row would get around that but the path estimate and metrics were not the same or complementary as they came from different states. Preserving all the possible states unique or complementary with their metrics and path estimates was the way to ensure all trellises were considered.

Unlike the conventional VA, here each trellis had its own CIR estimate, this meant the algorithm would try to match the trellis to the received sequence by finding a CIR that made them fit, how this happened depended on the order of the estimate as described in Section 3.3 and one type of match that caused errors is discussed in Section 3.5. by considering the mis-adjustment of the CIR.

Computational requirements were shown in Appendix D; the structure was made of parallel calculations of metric and CIR updating for each state, then sorting was

required. The choice of the LMS step to avoid instability was set for all the simulations at 0.1, and was briefly addressed in Section 3.6.

At the very beginning of the DSA an exhaustive search was made whilst the trellis filled to $O + \log_2(2M)$ samples long. If the CIR had been known the metrics should have indicated the correct trellis, since this was a blind estimation this time was used to start the training of the CIR. During the exhaustive search period all possible trellises are present, including the correct and delayed versions of it, called slipped here. Then trellises started to be discarded, but the correct and slipped versions were not compared to each other because they would be different states, unless the correct trellis had a sequence of $O + 1$ identical data. This was especially serious if the trellis with no slip delay was lost but two survivors are those with slip +1 and -1 sample period. With the CIRs chosen for simulations the coefficients lost from slip +1 and -1 contributed the same error to the metric. The correct trellis with no slip may be lost at the beginning of the algorithm because the errors from the first samples may be large while the LMS is learning and may be larger than those errors from another trellis. That other trellis would have a different estimated CIR so it would be unlikely to continue to give good approximations of the following received samples.

As the DSA continued it would have been good to continue to have $2M$ different trellises compared per state however as shown in Section 3.4 this was not the case and the effectiveness of this algorithm against fading was questioned.

2.1.4 Steps in the simulation sequence

Each simulation was made of various trials, and each trial used the same data to generate signals arriving at both antennas. In Table 2.1.4.1 the variables initialized for each simulation are shown.

$O = 5$	The estimated CIR order was the same as the true order, for CIR1 and CIR2 of Section 3.1.
$M = 4$	Reported as a good compromise between exhaustive search size and good performance in finding correct CIR reported by Seshadri [Ses94].
$\mu = 0.1$	As used by Seshadri.
$N = 10 \ O = 50$	10 times the model order is the usual upper limit for VA convergence.
EXBW = 25 %	A compromise between bandwidth efficiency and distortion introduced by the CIR.
number of data samples to generate = 1200 + 50 + 36 = 1286.	1200 was the number of bits expected to be within the coherence time, see Section 2.1.2. 50 was the length of the trellis which was the delay from starting the algorithm to getting the first data out. 36 was a delay introduced to allow the transmit and receive filters to pass a significant portion of the signal.
number of trials = 30	See Section 3.6
S/N = [3, 6, 8.5, 10, 12.5, 15, 20, 30]	Sequence covered interesting portion of BER performance.
Trellis	Matrix initially all zeros of size $2M2^O \times N$, filled with +1s or -1s.
Metrics	Matrix initially all zeros of size $2M2^O \times N$, filled with real numbers.
CIR estimate	Matrix initially all zeros of size $2M2^O \times O$, filled with complex numbers.

Table 2.1.4.1 The values used for the experiment in Section 3.2

All the signals were complex, although the data only had a real part, corresponding to BPSK.

For each trial using a particular S/N value:-

A. Put data through complex baseband model for each CIR:-

- a. A data sequence for this trial was generated and stored for checking performance later. The data was generated by random selection of +1 or -1.
- b. The data sequence was up sampled by two using insertion of one zero between each +1 or -1.
- c. The up sampled sequence was passed through the square root cosine TX filter, see appendix A for this filter's details.
- d. The filtered data sequence was then filtered by the CIR taken as a FIR filter. This gave the distorted signal arriving at the RX antenna, see appendix E for some eye diagrams.
- e. To apply the correct noise power and set the signal power as described earlier the distorted signal power was measured and an adjustment made by multiplying each sample by a correction factor.
- f. A noise sequence of length 2×1286 was generated using Gaussian distributed samples of mean zero and variance one, this sequence was filtered by the TX filter, the output of which was used to find the initial noise power which was adjusted to achieve the required S/N for this trial.
- g. Distorted data and noise were added together sample by sample to create the signal entering the RX.

- h. The receiver filter was used on the signal entering.
- i. From the output of the receiver filter down sampling by a factor of two produced the sequence supplied to the algorithm, and it was stored for use with the DSA, so the DSA had the same values to work on.

Each down sampled signal was used to drive the algorithm for each CIR wanted and the diversity combination of them:-

B. Exhaustive search segment

1. Start with sample 36, see delay comment above, the error between the received signal sample r and the estimated signal was found, $error_i = r - \hat{r}_i$, where i was the index to the row in the trellis matrix. The estimated signal \hat{r} was found for each of the $2M2^O$ trellises by using the current CIR estimated for that trellis and the state. $\hat{r}_i = \sum_{j=1}^O CIR_i(j).state_i(j)$. If the DSA was being used the error from the signal at the other antenna was also found using the CIR estimates for that antenna but the same candidate sequences.
2. In the exhaustive search segment the trellis was being filled by starting with one column filled by +1 in the top half and -1s in the rest. At each sample another column was appended, and a column of zeros removed from the other end. The columns appended were filled with +1s and -1s, $2M2^O$ long, so that all possible combinations were finally present after $O + \log_2(2M)$ samples.
3. The metric for each $2M2^O$ trellises was found by taking the product of the error and it's complex conjugate. For the diversity combination the products of both

errors was added, see Section 2.2. This column of metrics was concatenated to the Metrics matrix, and a column of zeros removed from the other end.

4. Using the errors each CIR estimate was updated by the LMS algorithm,

$$CIR_i(n+1) = CIR_i(n) + \mu \cdot \sum_{n=1}^O error_{in} \cdot state_{in}, \quad (2.1.4.1)$$

the CIR for each antenna in the DSA were updated with their own errors but the same state.

5. This sequence 1 to 4 was repeated for $O + \log_2(2M)$ samples, while the trellis matrix was still filling up, then trellises had to be discarded.

C. Fill trellis segment

6. For each row in the metric matrix the sum was found, which was the accumulated metric as required from Section 2.2.
7. The debugging was made easier by keeping the trellises in order, with all $2M$ of those in state 1 1 1 1 1 at the top down to the $2M$ trellises of state -1 -1 -1 -1 -1 at the bottom of the matrix. In practice it may have been more computationally efficient to just use pointers. Then the indices to trellises were sorted according to their accumulated metrics and the M indices with lower metrics identified. Those indices were then placed in a column matrix indicating where the state they represented would go in the next step of the trellis. The rows of the three matrices, Trellis, Metrics and CIR estimate were then swapped into position for the next step. To fill the trellis a column of new data for each state was appended and a column of zeros removed.

8. With the next received sample the error was found as in the exhaustive search segment.
9. Metrics were calculated as in the exhaustive search segment.
10. CIR updates were made as in the exhaustive search segment.
11. This sequence 6 to 10 was repeated for N samples until the trellis and metrics matrices were full non zero values.

D. Get data segment

12. The differential data output d_{out} was taken by looking at the two oldest values in the row of the Trellis matrix that had the lowest accumulated metric of all the rows. If the values were the same a 1 was appended to the data out matrix if not a zero was appended.
13. Steps 6 to 12 were repeated until all the samples in r were used.

E. Check differential data segment

14. The data stored from step a of the complex baseband model was converted to a differential sequence d_{in} .
15. By using convolution of the two differential data sequences d_{in} and d_{out} the best offset between them was found, see Sections 3.5 and 3.6 for a discussion of why this was required. The convolution showed a peak and the difference between the sample number of the peak and the center of the convolution gave the offset.
16. The number of correct data bits recovered was found by comparing bit by bit the two sequences using the best offset. Where an error was discovered its index in

the sequence was stored for investigation and the total number of errors for this trial was returned.

Segments A to E were repeated for another CIR and then the same down sampled signals from both CIRs were used to drive the DSA with segments B to E. For that trial the results for the total number of errors for each CIR alone and the DSA were stored.

This was repeated for the number of trials set for the S/N being used, then with the total number of errors for each of the trials an average BER was plotted for each CIR alone or the DSA on the Figures of BER versus S/N.

For the next S/N value all the above was repeated again to create the curves for each CIR alone and the DSA.

2.2 Incorporation of diversity

2.2.1 Derivation of metric calculation.

By considering the probability of the transmitted candidate sequence when the received sequences from the antennas were those sampled, the most probable was selected,

$P(\text{true transmitted sequence} = \text{candidate sequence} \mid \text{receive sample estimates for candidate CIR to antenna 1} = \text{received samples from antenna 1} \cap \text{receive sample estimates for candidate CIR to antenna 2} = \text{received samples from antenna 2})$.

$$\text{Using the Bayes' rule } P(Tx = S \mid r = r_1) = \frac{P(r = r_1 \mid Tx = S)P(Tx = S)}{P(r = r_1)}, \quad (2.2.1.1)$$

where Tx was the transmitted sequence, S was the candidate sequence or trellis and r_1 was the received sequence at antenna 1. Thus the comparison could be made in terms of received signal sequences given transmitted sequences. There were two observations that simplify the comparison of the set of candidate sequences, first the probability that the received sequence r_1 is $P(r = r_1)$ was the same for all the candidate sequences and so makes no difference and could be ignored. Second the candidate sequences in the set were all different but the probability of transmitting any one was equal to the probability of transmitting any other by definition so for the purposes of comparison $P(Tx=S)$ could also be ignored. These observations left $P(r=r_1|Tx=S)$ to be compared for all candidate sequences, and in this case there were two antennas so the comparison was for $P(r=r_1 \cap r_2 | Tx=S)$.

Since the receiver had no memory the probabilities for each sample in the sequences could be separated,

$$P(r = r_1 \cap r_2 | Tx = S) = P(r = r_{11} \cap r_{21} | Tx = S_1) P(r = r_{12} \cap r_{22} | Tx = S_2) \dots P(r = r_{1N} \cap r_{2N} | Tx = S_N), \quad (2.2.1.2)$$

where N was the number of samples in the truncated sequence. Then assuming the antennas were arranged to give uncorrelated samples the probability can be split into:-

$$P(r = r_1 \cap r_2 | Tx = S) = P(r = r_{11} | Tx = S_1) P(r = r_{21} | Tx = S_1) P(r = r_{12} | Tx = S_2) P(r = r_{22} | Tx = S_2) \dots P(r = r_{1n} | Tx = S_n) P(r = r_{2n} | Tx = S_n). \quad (2.2.1.3)$$

Assuming that the effect of all the corruption on the wanted signal was Gaussian noise the terms could be expanded in the form:-

$$P(r = r_{1i} | Tx_{1i} = S_{1i}) = \frac{1}{\sqrt{2\pi}\sigma_n} \exp\left(\frac{-(r_{1i} - S_{1i})^2}{2\sigma_n^2}\right), \quad (2.2.1.4)$$

here S_{1i} was the mean or noise-less sample at time i from passing that transmitted sequence through the CIR. This value was found by applying the candidate sequence to the estimated CIR for that candidate. Since all the terms had the $\frac{1}{\sqrt{2\pi}\sigma_n}$ factor it did not need to be considered in the comparison. Now the probability contained a product of exponentials, taking natural logs of both sides of the comparison allows it to be written as the sum of the terms:-

$$\begin{aligned} \ln[P(r = r_1 \cap r_2 | Tx = S)] = \\ \left(\frac{-(r_{11} - S_1)^2}{2\sigma_n^2}\right) + \left(\frac{-(r_{21} - S_1)^2}{2\sigma_n^2}\right) + \left(\frac{-(r_{12} - S_2)^2}{2\sigma_n^2}\right) + \left(\frac{-(r_{22} - S_2)^2}{2\sigma_n^2}\right) + \quad (2.2.1.5) \\ \dots \left(\frac{-(r_{1n} - S_n)^2}{2\sigma_n^2}\right) + \left(\frac{-(r_{2n} - S_n)^2}{2\sigma_n^2}\right). \end{aligned}$$

By definition a probability was less than or equal to one so the natural logarithm was zero or a negative number, as indicated by the negative signs in $-(r_{11} - S_1)^2$, to get the best possible probability the sum should be nearest zero which meant that the choice would be for the candidate sequence with the maximum total sum of $-(r_{11} - S_1)^2$ terms.

Since all the terms have the minus sign this could be ignored in the comparison and the minimum total sum used. The result could conveniently be used in a recursive routine by adding together the squared errors of each sample at both antennas. This could be extended to multiple antennas by simply adding all the errors squared to get the overall metric at every sample.

2.2.2 Different orders for each path

The estimated CIR order did not have to be same for both antennas, because the number of trellises, which were candidate transmitted sequences, depended on the order of the CIR the larger order would set the size of the matrices to be handled. However the metric combined both of the antenna metrics by adding the errors as shown above but there would not have been the same number of metrics to sum. This could have been overcome in two ways, illustrated in Figure 2.2.2-1, firstly keeping extra trellises per state to make up the difference in the smaller order calculation and using the metrics and estimated CIR from the extra trellises to improve the metrics by not discarding the information. Or secondly repeating those trellises, metrics and estimated CIRs selected to survive twice or more, matching the lower order candidate sequences to the last samples in the candidate sequences of the higher order trellis.

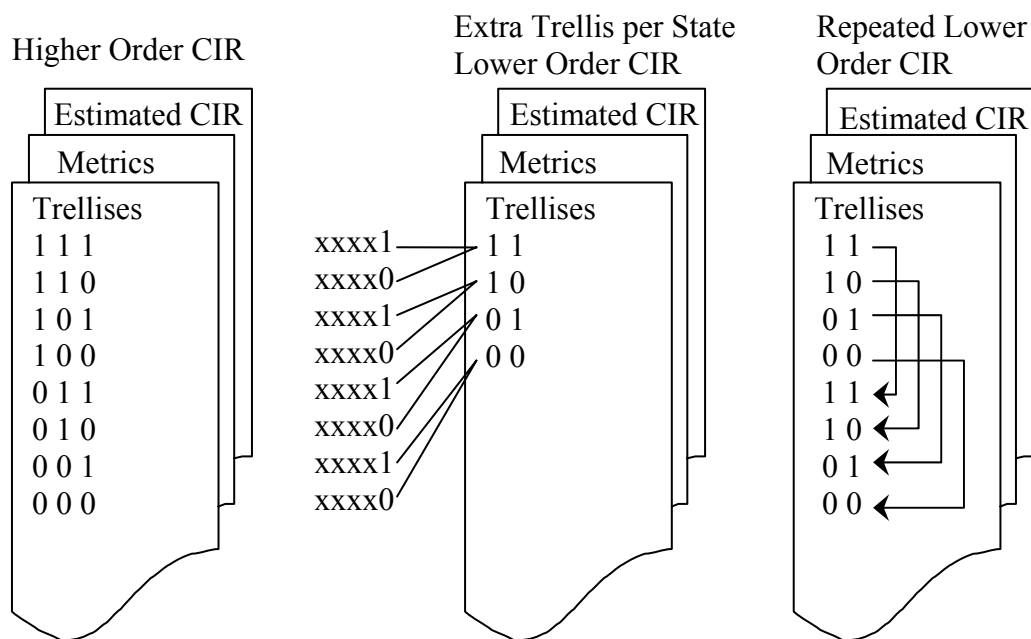


Figure 2.2.2-1 Illustration of how to deal with CIRs of different orders.

It would have been expected that the shorter CIR to converge faster than the longer one, if they had the same S/N ratio, so the most errors would have been caused from the longer CIR. This would have involved a more complicated simulation which may be required for further work in controlling the order of the CIR estimation. In Section 3.3 it was shown that as long as the estimated order was equal to that for either CIR good results could be achieved.

Chapter 3 Results of Computer Simulation of Single User Scheme.

3.1 Selection of channel impulse responses used for simulation.

The numerical simulation needed some CIRs to work with and four were chosen, shown in Figure 3.1-1, and tabulated in Table 3.1-1

CIR1	0.227 0.466 0.688 0.466 0.227
CIR2	-0.2 -0.5 0.7 0.36 0.2
CIR3	1.56+0.11i, -0.40-0.34i, -0.04-0.22i, 0+0.16i, -0.06-0.15i
CIR4	1 1 0 0 0 0.7

Table 3.1-1 Coefficients of the CIRs used for performance simulations.

The first two were used by Seshadri [Ses94] and Proakis [Pro83], the third was a randomly generated CIR with exponential roll off, the fourth was that recommended in the test specification [HRPD0032] for 1xEVDO for channel simulator configuration 4 in Table 11.4.1-1.

The third CIR was used to compare higher-order estimated CIR and the fourth one for comparing lower-order estimated CIR. Difficulty of CIR may be reflected by the presence of nulls in the frequency response, the spread of eigenvalues of the auto-correlation matrix, and inter-symbol interference shown by the impulse response.

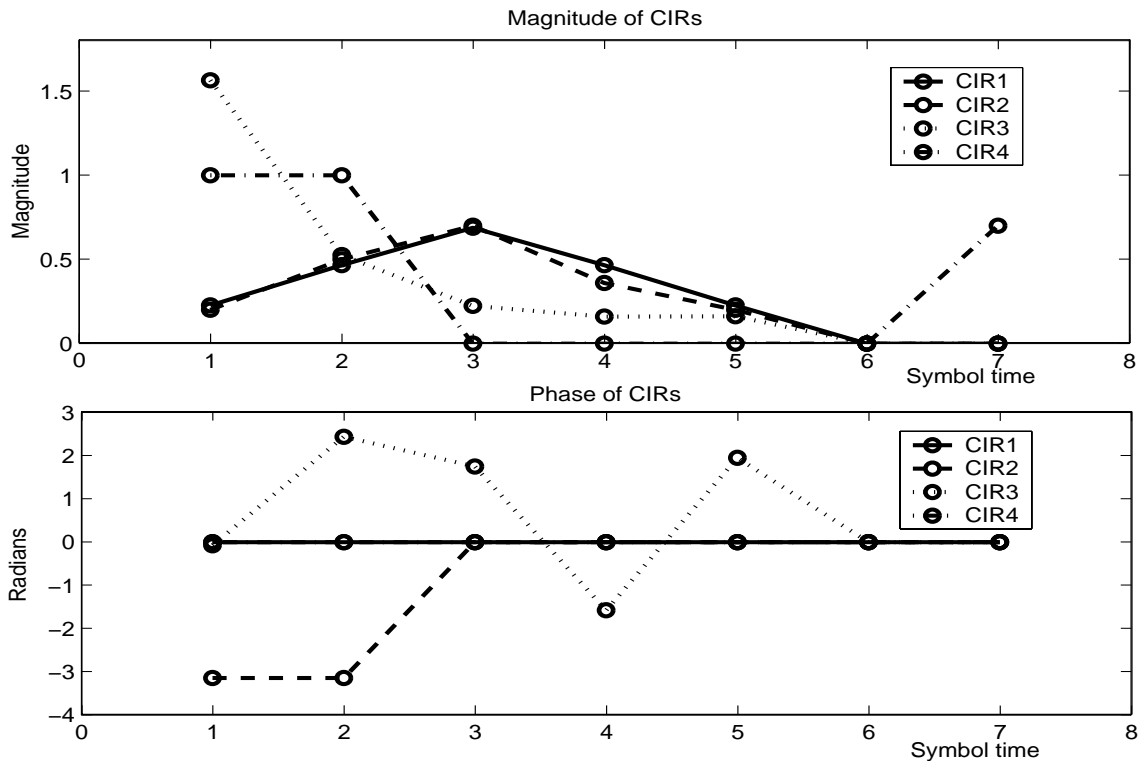


Figure 3.1-1 Channel impulse responses used for computer simulation.

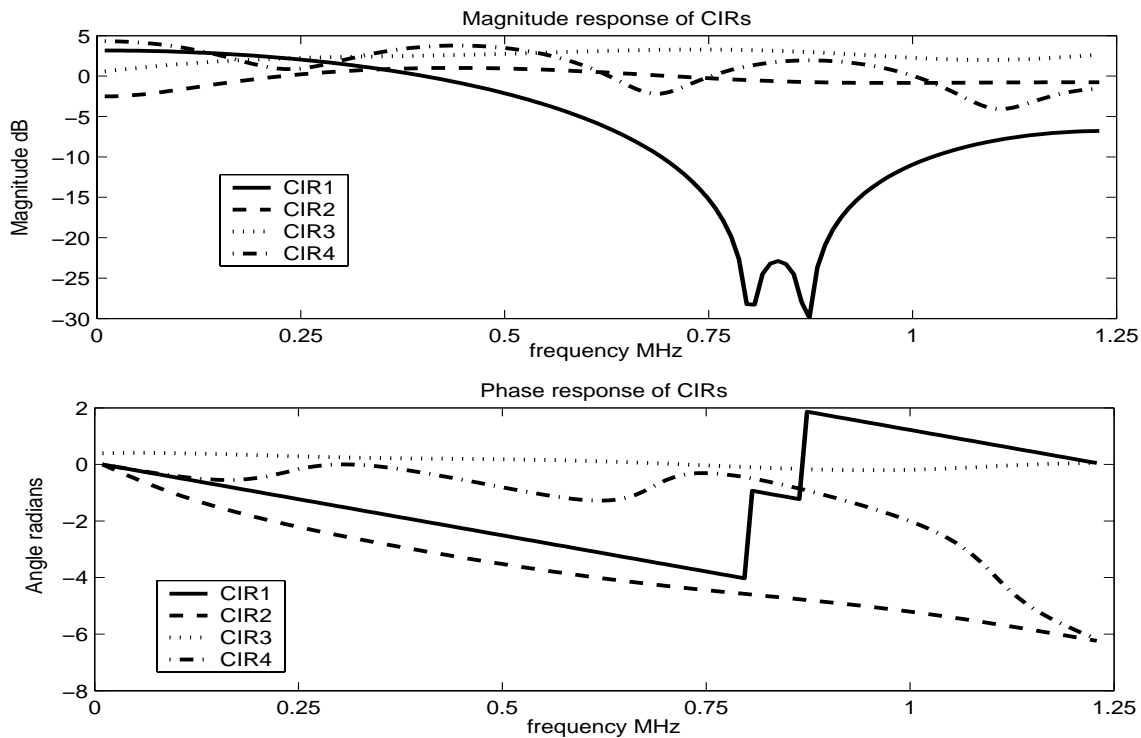


Figure 3.1-2 Frequency responses of CIRs used.

The frequency responses showed the presence of nulls and non-linear phase distortion of the CIRs. Figure 3.1-2 shows that CIR1 has a serious null, and CIRs 1 2 and 4 have phase distortion.

It appeared that noise was useful in reducing the eigenvalue spread, this was relevant to the time constant for convergence of the LMS algorithm that was used in the discussion of the convergence of all M trellises in Section 3.4.

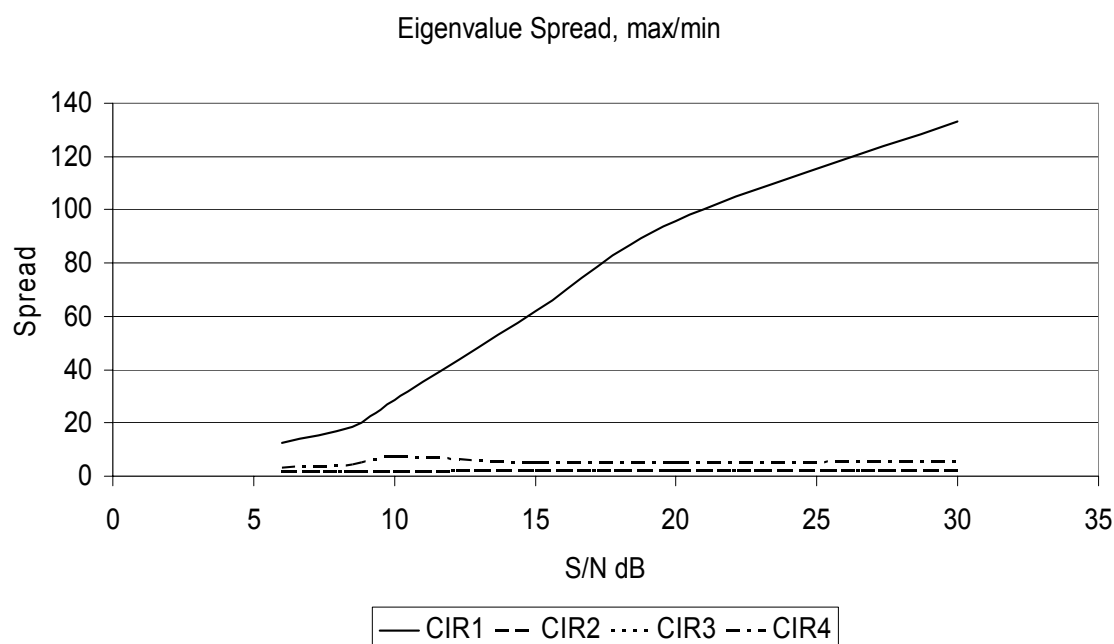


Figure 3.1-3 Eigenvalue spread of the CIRs used in the simulations.

As Haykin [Hay96] suggested a large eigenvalue spread of the correlation matrix R led to a directional convergence of the LMS algorithm, so in some trials it could be faster than other trials, this affected the performance, as shown in later sections. The CIRs chosen covered a range from reference CIR = 1 with spread of 1 to a spread of over 100.

Using pairs of CIRs for two diversity channels the correlation should be low according to the assumption in the definition of signal to noise ratio of Section 2.1.1, cross correlation coefficient ρ_c is given by,

$$\rho_c = \frac{E[r_1 r_2^*]}{\sqrt{E[|r_1|^2] E[|r_2|^2]}}, \quad (3.1.1)$$

where r_1 and r_2 the received signals. For CIR1 and CIR2 ρ_c was 0.42 and for CIR3 and CIR4 ρ_c was 0.40.

In the Appendices there were some more details of the CIRs; appendix E for eye diagrams of CIR2 and Appendix F for the zeros of the CIRs.

3.2 Consequences of the optimal combining of a second antenna.

Incorporating the combination of two path diversity as shown in Section 2.2.1 with the simulation as described in the steps of Section 2.1.4. The 1 antenna CIR2 trace in Figure 3.2-1 showed a peak at an S/N of 30 dB; this was the effect of two of the thirty trials having 122 and 194 errors which was significantly greater than the other trials by two orders of magnitude; these are due to slippage as described in Section 3.5. Similarly the two antenna CIR1 and CIR2 trace shows a peak at S/N equals 15 dB due to one trial with 58 errors. For a BER of 5×10^{-3} a 4 dB improvement over the better channel was achieved. Conventionally the overall gain due to diversity was the sum of two components, the combining gain due to two signals giving a 3 dB gain and the diversity gain. For these simulations diversity gain due to fading was not applicable. However, some improvement above 3 dB combining gain could be seen before the start-up and slip errors dominated creating a BER floor at higher S/N.

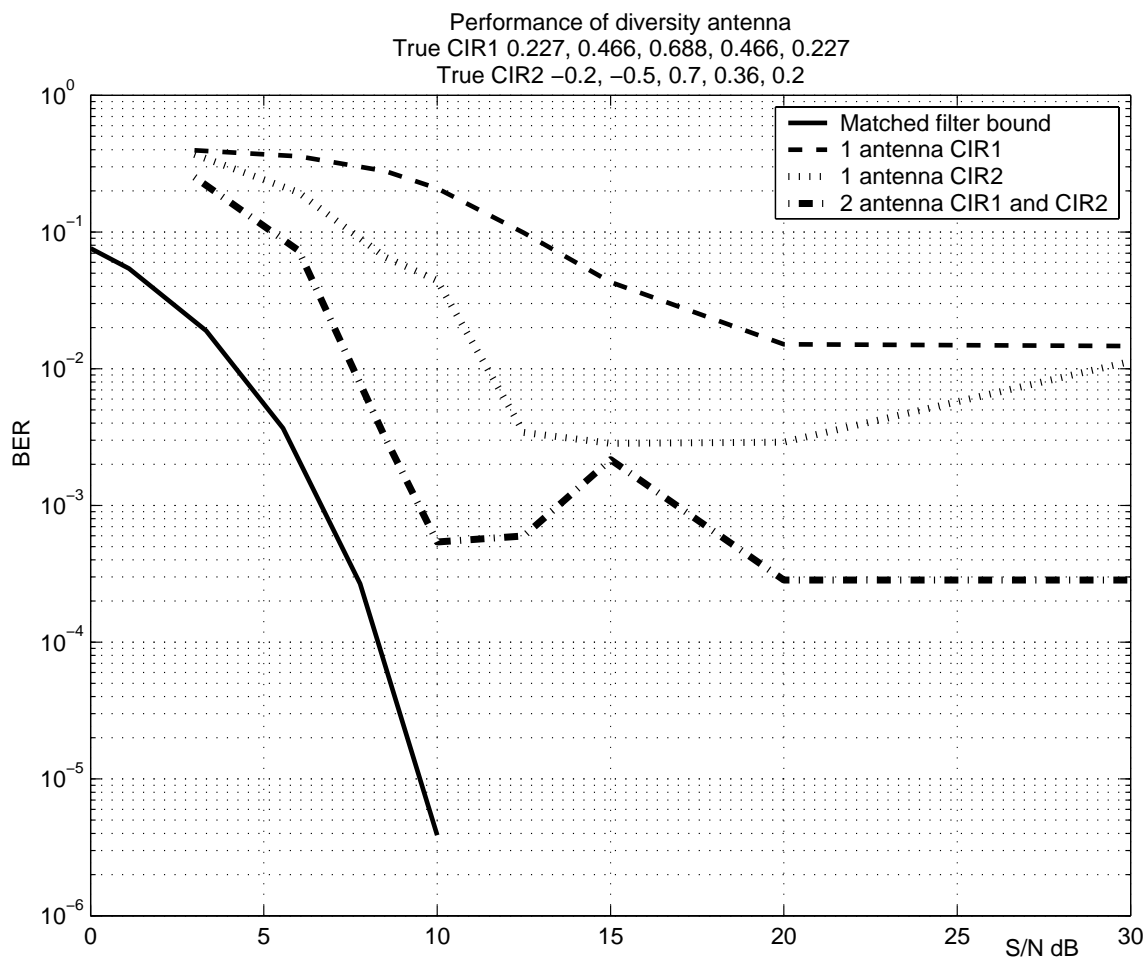


Figure 3.2-1 Improvement of BER performance by optimal diversity combining.

The most important characteristic of DSA should be its speed; this can be seen in Figure 3.2-2 by considering the first 100 data samples where the two antenna diversity produced better performance than either of the single channels alone. This plot was generated with the same data as Figure 3.2-1 the number of errors with indices less than 101 were also returned along with the total number of errors as described in Section 2.1.4.

To ensure the effect of the M trellises kept per state is included the start up was defined as the first 100 detected data, see Section 3.4, as a compromise between having the correct CIR learnt and not losing the effect of M trellises per state as well as having

a fixed size to do the comparison with. The use of diversity appeared to allow the detector to pick the correct trellis more quickly because it produced lower errors after learning for the same time. This was due to the way the metrics, made of the squared errors, are combined from both antennas, because the noise at each antenna is assumed to be independent the chances of both channels being corrupted at the same time is reduced.

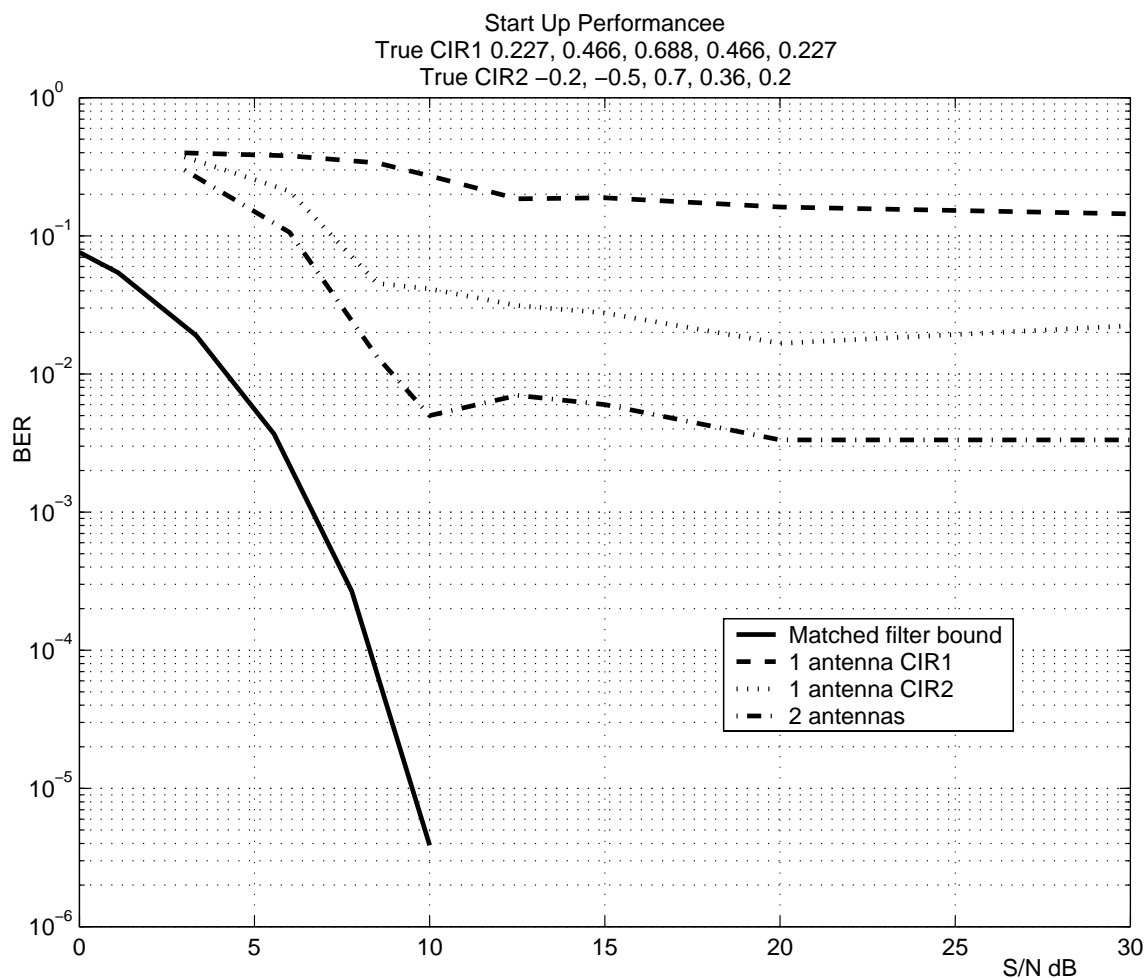


Figure 3.2-2 Start up performance with diversity.

The floor to the BER at higher S/N ratios may have been due to the slippage as described in Section 3.5 or if slippage was not the cause as there were only 100 samples per trial a few errors in each trial would suffice. For CIR1 the BER floor seemed to be about 0.2, for CIR2 the floor seemed to be 0.02 and for the diversity combination the

floor seemed to be 0.004. Those would correspond to CIR1 having 20 errors per trial, CIR2 having two errors per trial and the diversity combination four errors in every ten trials. The data detector considered the oldest sample in the trellis and even after ten times the CIR order, 50 samples, the data in all the trellises had not converged to be the same, as would be expected using the VA with a known CIR. This was because the selection of which trellis to keep is started when the number of samples collected is only $O + \log_2(2M)$. This was limited by the typical problem with this type of algorithm that was the number of computations needed as pointed out in Section 1.3. Therefore in the example plotted the first trellises were discarded after $5 + 3 = 8$ samples are received. To survive after these eight samples the correct trellis should have had a lower accumulated metric than four out of the eight trellises that are compared at the state. So the correct trellis made a better estimate of the CIR than four of the eight to get a lower error for the estimated received signal. Thus the noise did not distort the received signal too much to drive the error higher at the eighth sample or the noise did not drive the estimated CIR away from the true one during the previous seven samples. Using the LMS algorithm to find the CIR only seven samples would not have been expected to be sufficient to get a good estimate of the true CIR however this was not what was used, rather the accumulated metric only has to be lower than most of the other trellises leading to state. This would be expected to be true since using the wrong training sequence for the LMS algorithm should produce the wrong CIR which in turn produced the wrong estimate of the received sample in turn leading to larger error and larger accumulated metric.

When the first samples were received and the LMS algorithm started to learn the CIR the initial coefficients are all zeros and noise on the first samples pushed the

estimate of the CIR for the correct trellis away from the true CIR leaving another trellis with a lower accumulated metric, by definition any other trellis had at least one error. In Figure 3.2-3 the distribution of errors over the sample number was shown and there were indeed significantly more errors at the beginning of the trials. The simulation as described in Section 2.1.4 was changed to fix the S/N as 15 dB using only CIR2 and returning the index of the errors for 100 trials. The error indices were then grouped into bands of 20 wide to plot on the histogram.

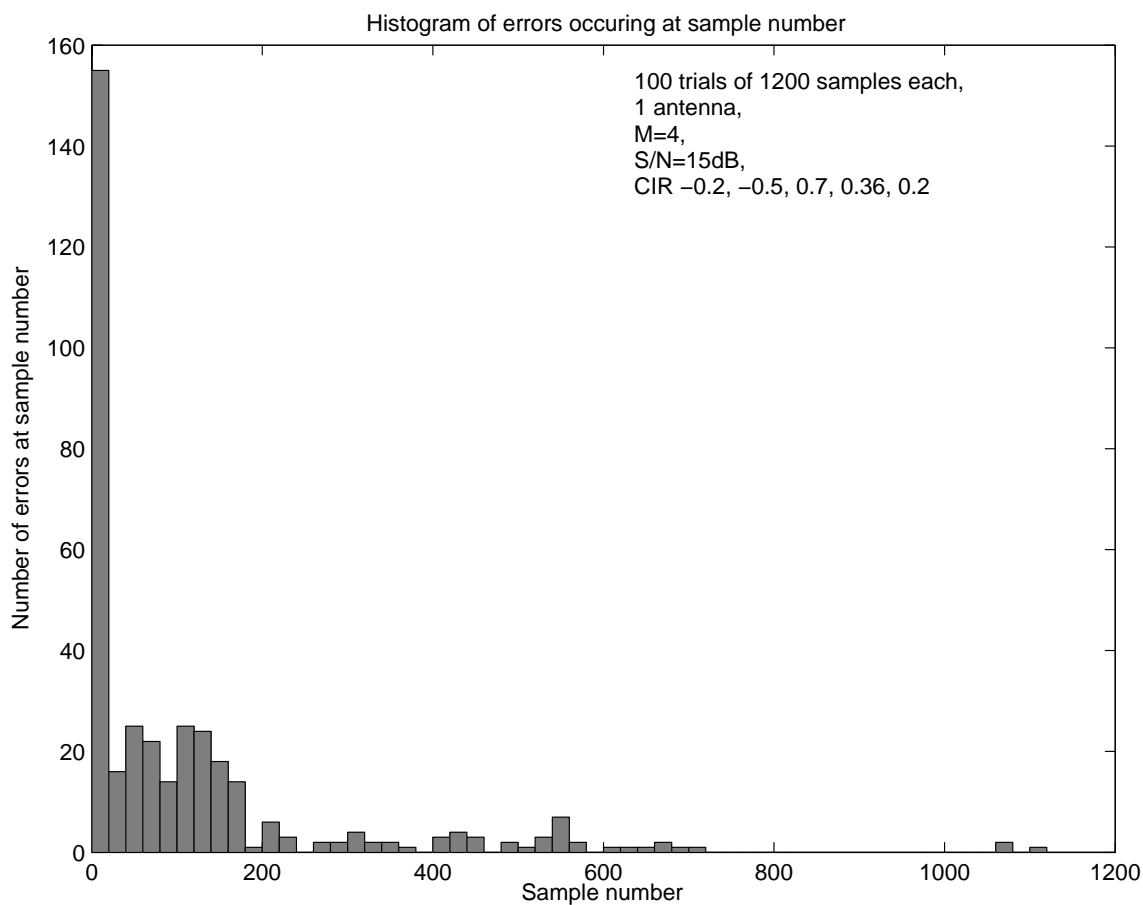


Figure 3.2-3 Distribution of errors over length of trial.

3.3 Effect of model order mismatch, between the true and estimated model.

Since the receiver was unlikely to know the correct CIR the effect of the mismatch between the true and estimated CIR order was investigated and found to be significant. The simulation as described in Section 2.1.4 was changed slightly to fix the S/N at 15 dB for all trials but vary the O parameter, the results were stored and averaged to give the following Figures in the same way as when the variable was S/N.

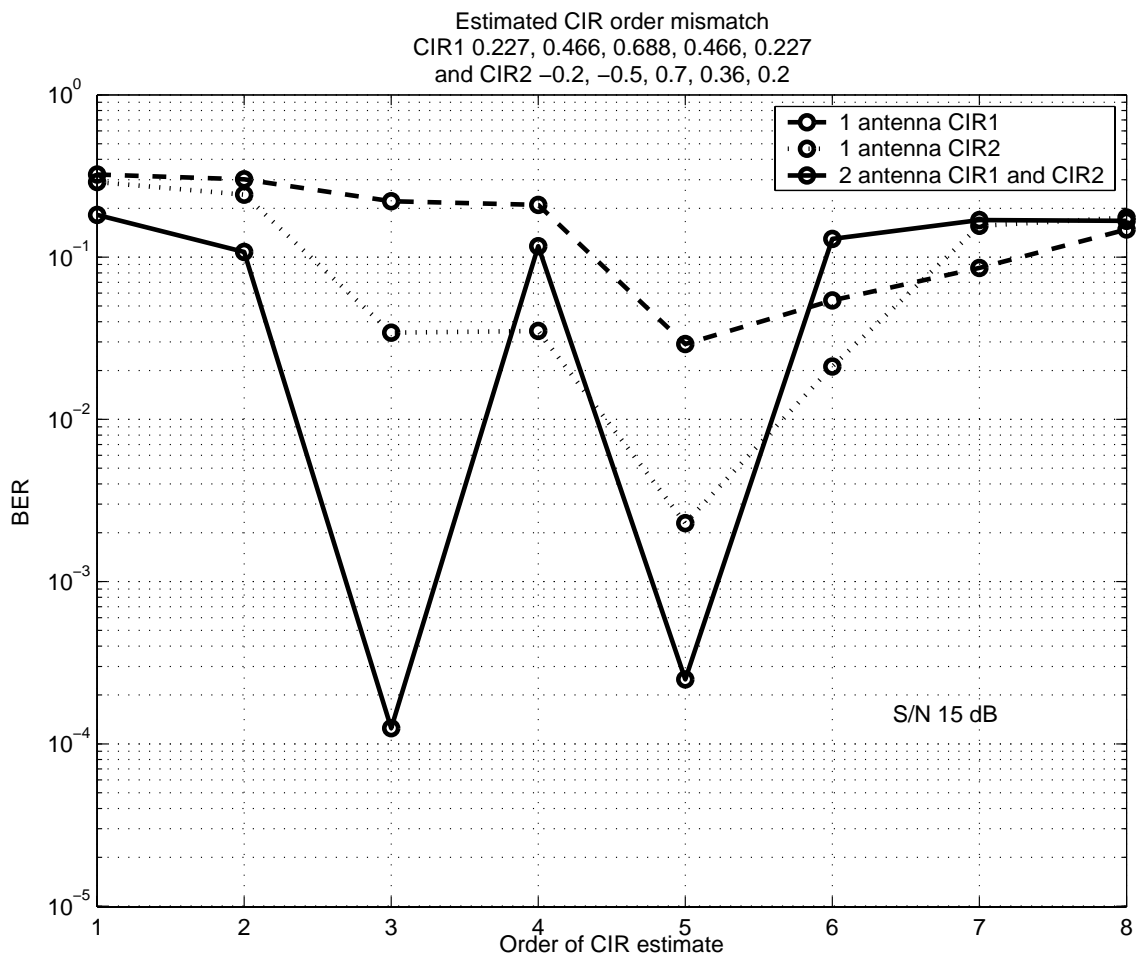


Figure 3.3-1 Performance of mismatched orders when the true order was five.

When the true orders of the CIRs were equal the addition of the second antenna improved the performance to be better than either of the two antennas taken alone, as seen in the previous section. If the order of the estimated CIR was higher than the true order the performance was drastically reduced, this was due to slippage as described in Section 3.5. The improvement in diversity performance with a third-order estimate was due to the relation between the true fifth-order response of CIR2 and the close approximation to it by a third-order estimation, which happened to be $[-0.5 \ 0.7 \ 0.36]$ the middle three coefficients .

The third order estimation of CIR2 seemed to give a sufficiently good guide to push the estimation of CIR1 to a better estimation than it could find alone because the same trellis was used for each path with this diversity combining technique. I think it was chance that turned up this result and the probability of having a CIR that could be well modelled by a lower order may not be high, also the problem remained to find the correct lower order, this was suggested as further work in Section 4.2. However it would have been an advantage for the diversity technique.

Another example of finding the right lower order model was illustrated by the randomly generated CIR in Figure 3.3-2. Here a first or second order CIR estimate was sufficient and in fact using the true order with S/N of 15 dB produced more errors. Since the DSA chose the lowest accumulated metric from all the possible states it was sufficient for the lower order CIR estimation with the correct trellis to give better estimates of the received signal than the incorrect trellises because the incorrect trellises have driven their CIR estimates away from the optimum and so their estimates of the received signal to worse values.

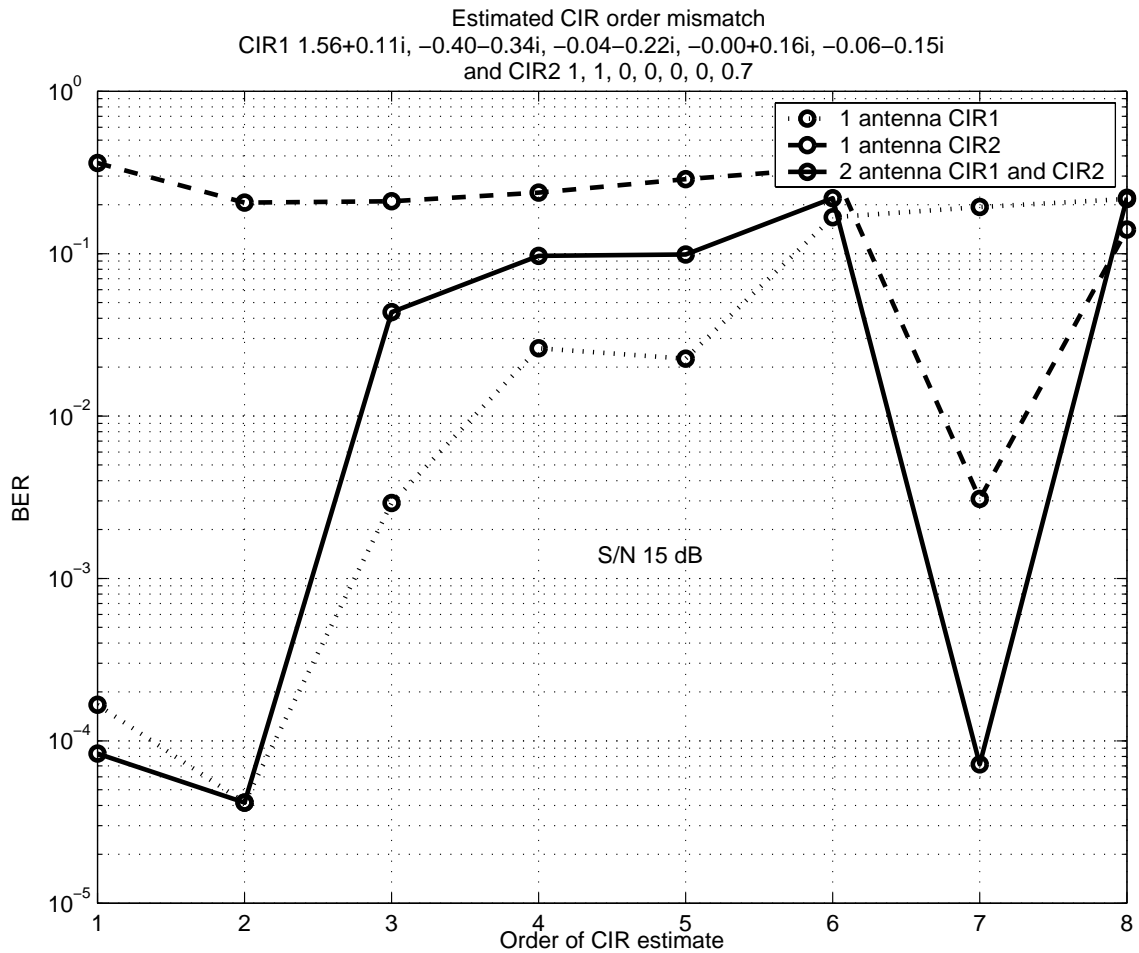


Figure 3.3-2 Performance with different true CIR orders.

The most significant other trellis was the correct one but slipped one sample period as described in Section 3.5. Therefore the slipped CIR would have lost coefficients that had larger magnitudes which led to larger errors in estimates of received sample. The expected error after learning the CIR as in Section 3.5 was,

$J = J_{\min} + J_{ex}(\infty)$, to which was added the error from the omitted CIR coefficients which make up the error in the estimation, and the received noise variance was added to find the total mean square error,

$$MSE = J + \sum_{i=0+1}^L CIR_i CIR_i^* + \sigma^2, \quad (3.3.1)$$

where MSE was the mean squared error, and σ^2 was the noise variance. Assuming the best possible CIR was the one with the largest CIR coefficients in it, and the second best was the slipped version. By comparing the errors from the best possible CIR and the second best some indication of the chances for making an error could be gained.

S/N 15 dB	CIR2 -0.2 -0.5 0.7 0.36 0.2	
Order	$MSE = J + \sum_{i=0+1}^L CIR_i CIR_i^* + \sigma^2$ best possible CIR	$MSE = J + \sum_{i=0+1}^L CIR_i CIR_i^* + \sigma^2$ second best CIR
5	0.047	0.087
4	0.087	0.087
3	0.127	0.217
2	0.257	0.377
1	0.507	0.747

Table 3.3-1 Mean errors for various estimated CIR orders using CIR2.

In Table 3.3-1 the orders with best possible CIR error about half the second best CIR error had much better BER performance than the others which had the second best CIR error closer to the best one. The fourth order case had the same errors, one CIR was [-0.2 -0.5 0.7 0.36] and the other [-0.5 0.7 0.36 0.2]. Because the coefficients were the same at the beginning and the end, the errors from omitting one or the other are the same and performance is limited by slip errors.

For CIR1 in the order 3 line of Table 3.3-2 the assumption that the best CIR was the largest was not true, it could converge to something like [0.6 0.6 0.45] which had a similar frequency response and would switch between this and [0.49 0.68 0.46].

S/N 15 dB	CIR1 0.227 0.466 0.688 0.466 0.227	
Order	$MSE = J + \sum_{i=0+1}^L CIR_i CIR_i^* + \sigma^2$ best possible CIR	$MSE = J + \sum_{i=0+1}^L CIR_i CIR_i^* + \sigma^2$ second best CIR
5	0.043	0.095
4	0.095	0.095
3	0.146	0.311 2 cases
2	0.363	0.363
1	0.580	0.837

Table 3.3-2 Mean errors for various estimated CIR orders using CIR1.

In the case of CIR3 where the best possible CIR error was half or less than the second best good performance was found in the BER plot of Figure 3.3-2

S/N 15 dB	CIR3 1.56+0.11i, -0.40-0.34i, -0.04-0.22i, 0+0.16i, -0.06-0.15i	
Order	$MSE = J + \sum_{i=0+1}^L CIR_i CIR_i^* + \sigma^2$ best possible CIR	$MSE = J + \sum_{i=0+1}^L CIR_i CIR_i^* + \sigma^2$ second best CIR
5	0.143	0.169
4	0.169	0.194
3	0.194	0.243
2	0.243	0.521
1	0.521	2.703

Table 3.3-3 Mean errors for various estimated CIR orders using CIR3.

S/N 15 dB	CIR4 1 1 0 0 0 0.7	
Order	$MSE = J + \sum_{i=0+1}^L CIR_i CIR_i^* + \sigma^2$ best possible CIR	$MSE = J + \sum_{i=0+1}^L CIR_i CIR_i^* + \sigma^2$ second best CIR
7	0.119	0.609
6	0.609	0.609
5	0.609	0.609
4	0.609	0.609
3	0.609	0.609
2	0.609	1.609
1	1.609	2.609

Table 3.3-4 Mean errors for various estimated CIR orders using CIR4.

This possibility of lower order modelling should be tempered by the final CIR, the mean errors in Table 3.3-4 for CIR4 showed that the true CIR order was required; this seemed to be because of the significant coefficients at the beginning and end of the CIR. In the case of order 2 I think the size of the error itself for the best CIR was the cause of the bad performance, rather than the relation to the second best CIR. However these four CIRs were only a selection from the whole range of possibilities and further work would be required to draw general conclusions.

Summarizing; use of the diversity combining technique could improve BER performance when the correct CIR was used, otherwise the performance may even be slightly worse than the single antenna techniques, and that performance was about 2 orders of magnitude worse than using the true CIR order.

3.4 Convergence of M trellises per state.

To avoid losing the correct data in the form of the correct trellis, only the M best trellises were saved for every state rather than an exhaustive search. Definition of convergence: when the M trellises of the state with the minimum accumulated metric were the same. Consequences of this may be the loss of correct trellis and so the performance would be lowered when fading occurred. Convergence happened in this manner, assuming $M = 4$ was chosen and $L = O = 3$, and letting 1 be the correct data and 0 be the wrong data, then considering only the state that had the correct data four trellises were chosen from the eight calculated. Assuming that the best metric would be from the correct trellis, and the second best metric from the trellis with the oldest incorrect data. The oldest incorrect data would have led to a lower accumulated metric than newer incorrect data in two cases, first where the CIR was being learnt the newer error could

have a larger error compared to an older estimate made with an inaccurate CIR, or second noise and the mis-adjustment of the CIR estimate in the newer error metric could have outweighed the older string of error metrics. The data in the last positions of the eight trellises would be,

$$\begin{array}{cccccc}
 1 & 1 & 1 & 1 & 1 & 1 \\
 1 & 1 & 0 & 1 & 1 & 1 \\
 1 & 0 & 1 & 1 & 1 & 1 \\
 1 & 0 & 0 & 1 & 1 & 1 \\
 0 & 1 & 1 & 1 & 1 & 1' \\
 0 & 1 & 0 & 1 & 1 & 1 \\
 0 & 0 & 1 & 1 & 1 & 1 \\
 0 & 0 & 0 & 1 & 1 & 1
 \end{array} \tag{3.4.1}$$

all the last three columns are ones as this was the same state which was the correct data.

The lowest metrics for trellises should correspond to these trellises which were chosen to survive, because they have only one error which could have driven the CIR estimates off target to increase the error in the next estimated sample,

$$\begin{array}{cccccc}
 1 & 1 & 1 & 1 & 1 & 1 \\
 0 & 1 & 1 & 1 & 1 & 1 \\
 1 & 0 & 1 & 1 & 1 & 1' \\
 1 & 1 & 0 & 1 & 1 & 1
 \end{array} \tag{3.4.2}$$

At the next sample these were joined in the correct state by some trellises from a state that had at least one error previously,

$$\begin{array}{cccccc}
 1 & 1 & 1 & 1 & 1 & 1 \\
 0 & 1 & 1 & 1 & 1 & 1 \\
 1 & 0 & 1 & 1 & 1 & 1' \\
 1 & 1 & 0 & 1 & 1 & 1
 \end{array} \tag{3.4.3}$$

from the correct state last sample. Joined with,

$$\begin{array}{cccccc}
 1 & 1 & 1 & 0 & 1 & 1 \\
 0 & 1 & 1 & 0 & 1 & 1 \\
 1 & 0 & 1 & 0 & 1 & 1' \\
 1 & 1 & 0 & 0 & 1 & 1
 \end{array} \tag{3.4.4}$$

where 0 1 1 was the state that must be the other previous state leading to the next state 1 1, at the next sample the correct state would therefore have trellises

$$\begin{array}{ccccccc}
 1 & 1 & 1 & 1 & 1 & 1 & 1 \\
 0 & 1 & 1 & 1 & 1 & 1 & 1 \\
 1 & 0 & 1 & 1 & 1 & 1 & 1 \\
 1 & 1 & 0 & 1 & 1 & 1 & 1 \\
 1 & 1 & 1 & 0 & 1 & 1 & 1' \\
 0 & 1 & 1 & 0 & 1 & 1 & 1 \\
 1 & 0 & 1 & 0 & 1 & 1 & 1 \\
 1 & 1 & 0 & 0 & 1 & 1 & 1
 \end{array} \tag{3.4.5}$$

here the trellises with the minimum and oldest errors were chosen to survive again.

These are the trellises which survived from the previous sample, but the position of the error has effectively moved back one place. If this were repeated 50 times the errors would have got to the end of the trellis that is stored and would then be lost, leaving the four trellises the same.

This did not happen so cleanly in practice as shown in Figure 3.4-1. The relation between S/N and convergence for a 5th order CIR with 5th order estimate is shown for CIR1 and CIR2 and compared to the DSA. The simulation as described in Section 2.1.4 was changed slightly return the sample number when all M trellises with the lowest accumulated metric were the same instead of the number of errors. This sample number was averaged and plotted for each CIR and the DSA. The two antenna case converges at lower S/N ratios but not any faster than the one antenna. Convergence happened in the shortest time around 10 dB S/N ratio which was reflected in the BER performance by the

S/N ratio where the BER stopped reducing and flattened off as S/N ratio increased. It would have been expected that the DSA would converge more rapidly as S/N increased which would have resulted in less noisy received samples and lower errors for the correct trellis following the average time constant for the LMS algorithm [Hay96]

$$(\tau)_{mse,av} \approx \frac{1}{2\mu\lambda_{av}}, \text{ where } \mu \text{ was the LMS step size set to } 0.1 \text{ for all the simulations and } \lambda_{av}$$

was the average eigenvalue of the received correlation matrix.

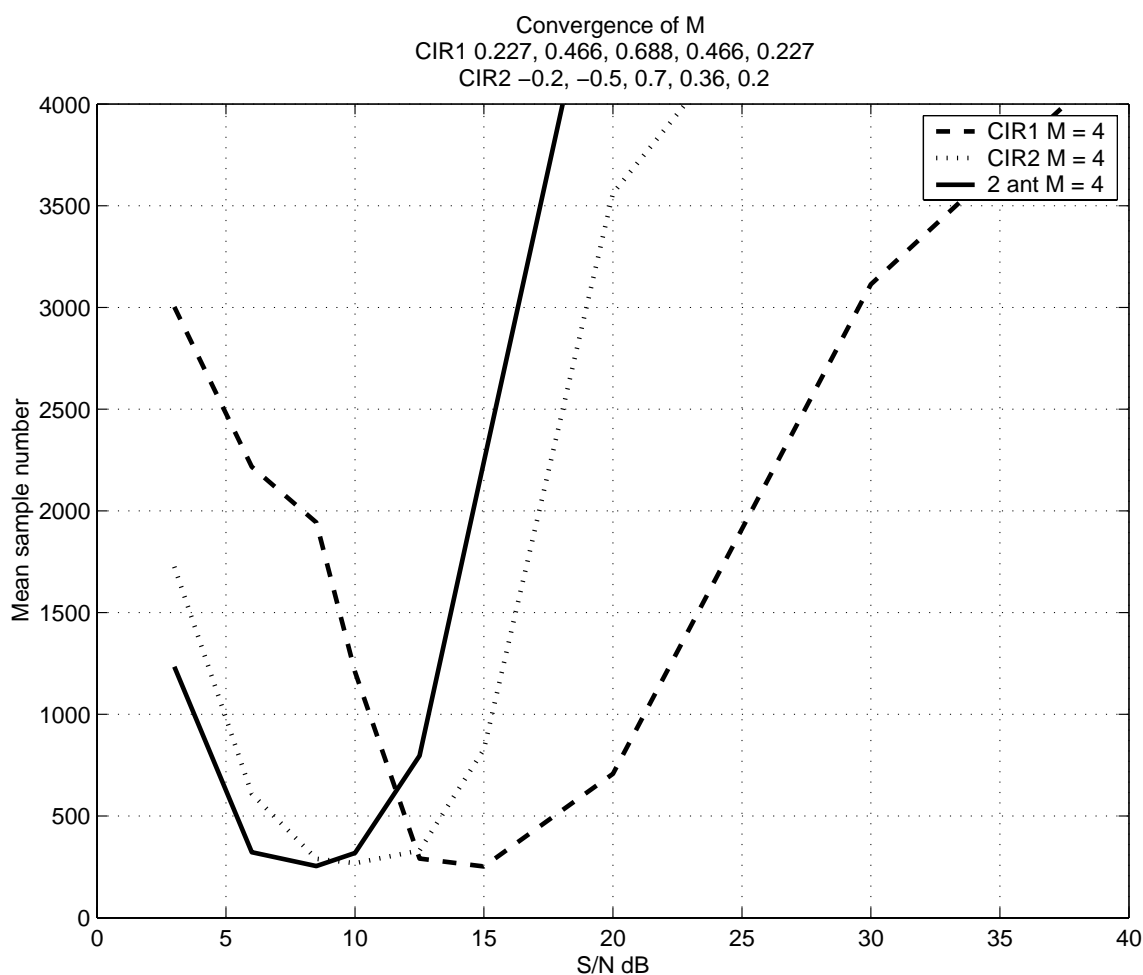


Figure 3.4-1 Convergence of all M trellises kept per state to the same trellis.

However there seemed to be another effect coming into play to increase the convergence time for the M trellises and that was trellises from the 0 1 1 state, if one of

these was surviving that would be sufficient for the M trellises not to converge. Before convergence at least one of the M trellises that came from the correct state had at least one error by definition. One error in the trellis would provoke a chain of larger errors in the estimation of the next sample as the error in the trellis worked its way through the CIR and the LMS tried to correct for it and then readjust as the correct trellis followed. So one of the M trellises had a string of larger metrics, which may have been placed much further away in the trellis.

The trellises from the 0 1 1 state also had a string of larger metrics but if it had the correct trellis leading up to that state the comparison is just about the difference in the two larger metric strings, and the newer error from the 0 1 1 state has only three (the length of the CIR) larger metrics compared to those during the correction of the CIR by the LMS algorithm in the correct trellis, so it would have been more likely to change to a trellis with a newer error, thus preserving a different trellis. For this to be true the metrics from the error in the trellis should dominate those when the correct trellis is used, this would have been the case when the estimated CIR was very close to the true one as expected at higher S/N ratios.

For the diversity case the easier to learn CIR seemed to be able to help the more difficult CIR learn by keeping the correct trellis as in the mismatched order Section 3.3.

Although the trellises were the same the metrics and path estimates were not the same but took some more time to equalize.

To compare the effect of using diversity to increasing the value of M Figure 3.4-2 showed how diversity improves performance at lower S/N and M can reduce the BER floor. The simulation as described in Section 2.1.4 was changed to add two extra sets of

results both with CIR2, one was with $M = 1$ and the other with $M = 16$. New data was generated for all five curves so they did not show the same slip errors as Figure 3.2-1. A trade off between computing M extra trellises and adding an extra diversity receiver could be made in this manner. The first 100 samples were used to avoid losing the M different trellises.

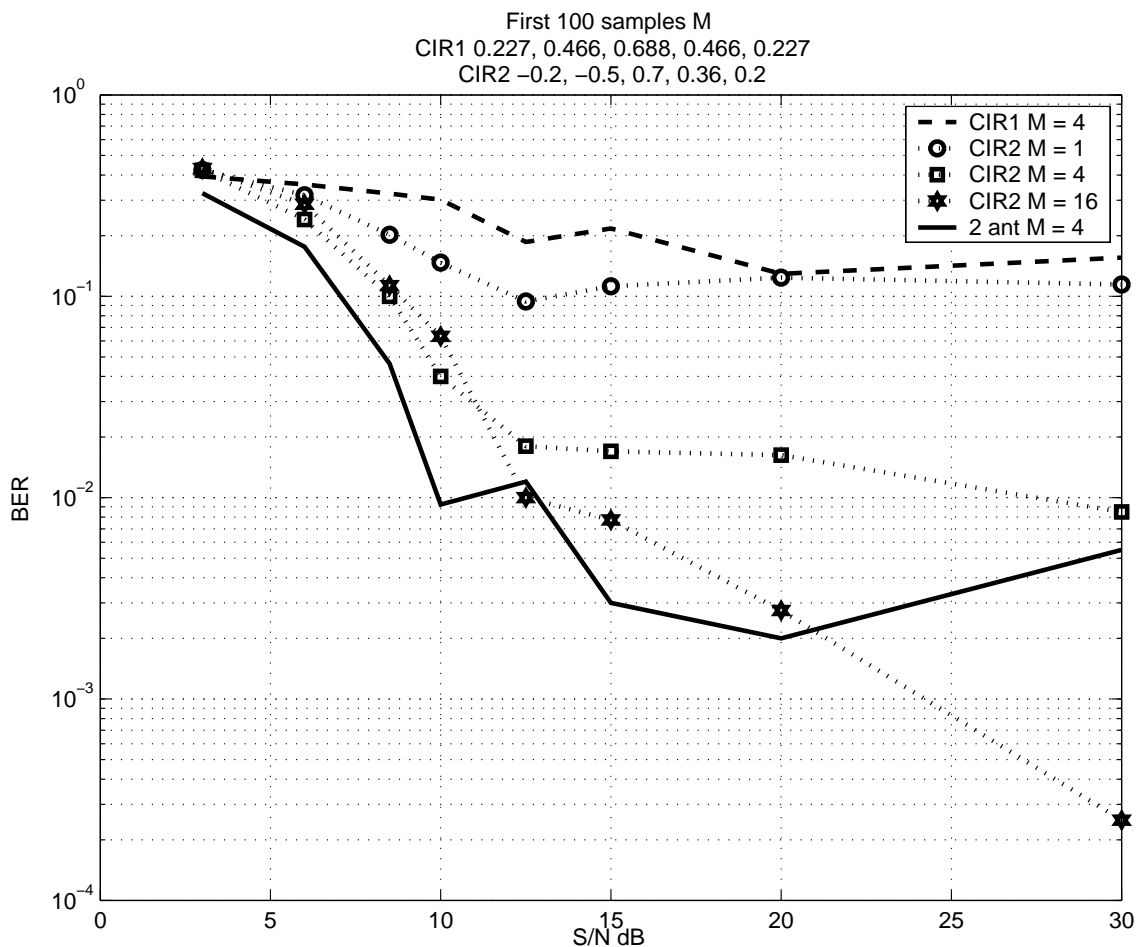


Figure 3.4-2 Comparing diversity to computing M trellises.

If the easier CIR was used with one antenna increasing M to 16 would achieve similar performance to a two antenna diversity with $M = 4$, one antenna would have required double the processing compared to two antennas which have double the hardware, but the diversity system still has better performance at low S/N ratios due to

the increased signal received. As M was doubled the exhaustive search increased by one sample allowing the CIR estimate of the correct trellis to converge, while the CIR estimates from the incorrect trellises stayed noisy, except for those slipped trellises described in Section 3.5.

3.5 Consideration of “slippage”.

Slippages were defined as the change in selection between two versions of the correct trellis, where the only difference in the versions was the delay by one sample period of one trellis compared to the other. The corresponding CIR estimates were also offset by one sample period. To illustrate this Figure 3.5-1 was from one trial showing the CIR which had the minimum accumulated metric at each sample time.

The trial was set up as in Section 2.1.4 using only one antenna, the true CIR was fifth order with coefficients $[-0.2, -0.5, 0.7, 0.36, 0.2]$, the S/N was 10 dB. The CIR corresponding to the trellis with the lowest accumulated metric was stored at each sample, a portion was displayed in the Figure with the corresponding data and the error. The horizontal axis was the sample index indicating time from left to right. The top row was the true transmitted data sequence. Row 2 was a sequence to indicate errors by 0 for good and 1 for bad. Row 3 was all zeros to separate the errors from the CIR coefficients. The estimated seventh order CIR was on rows 4 to 10, the magnitude only was displayed to avoid the confusion with the complements which were allowed, see Section 2.1.3. Following the colour change in the rows 4 to 10 to see when slippage occurred, from the left hand side the LMS algorithm was at the end of learning the CIR. The correct CIR had a peak indicated by orange colour for 0.7 in row 6, when the orange colour moved to row 7 a slip had occurred. It appeared that there was always a slip when there was an

error but not always an error when there was a slip. This was due to the data being compared actually being the same from a string of either +1s or -1s.

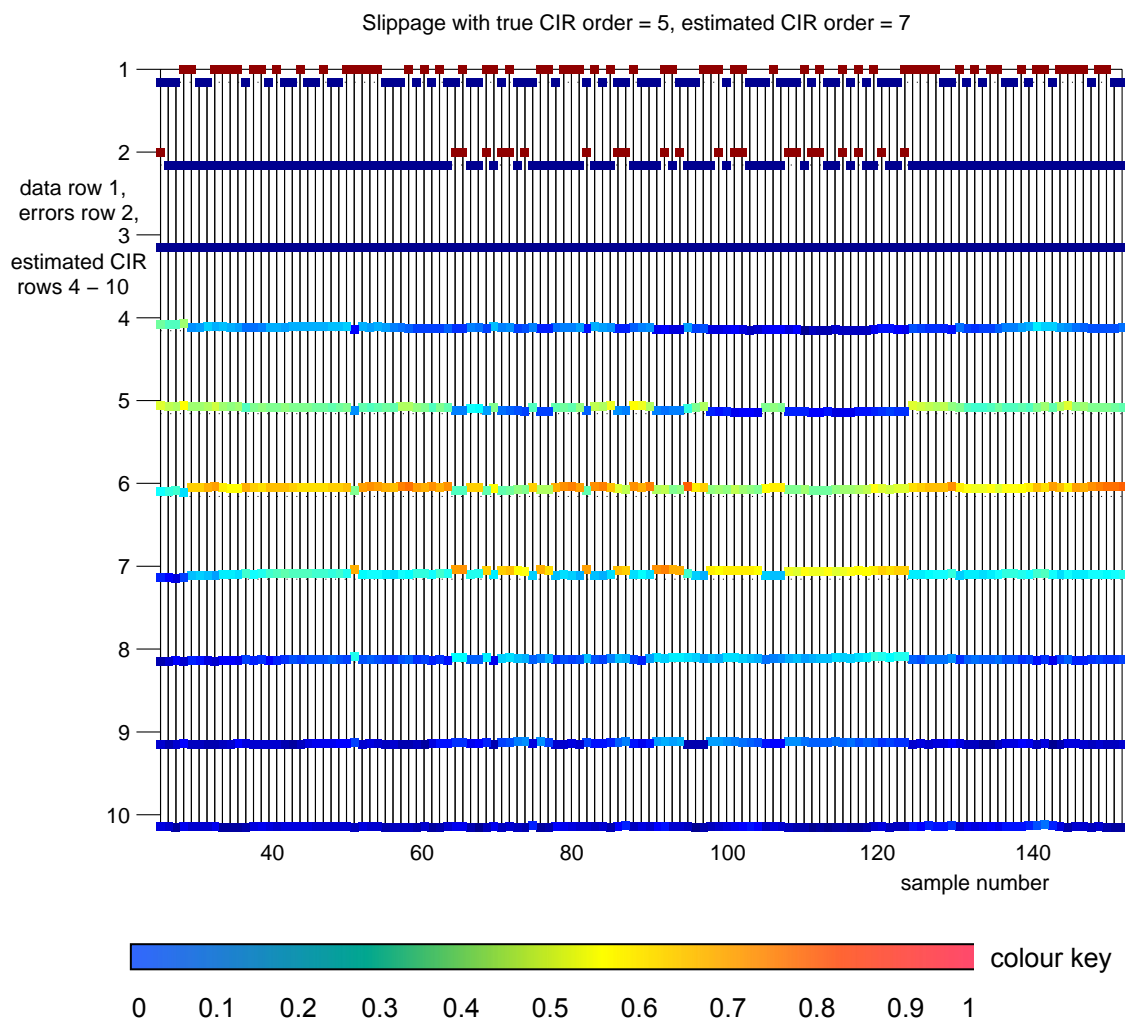


Figure 3.5-1 Illustration showing slippage in the CIR estimate.

It was easy to understand the way that the LMS algorithm could converge to both a slipped and non-slipped CIR when the estimated CIR order was greater than the true order, but the results from the BER simulations using the correct CIR order also showed this slip effect.

To illustrate the effect of slippage on the BER performance the number of errors per trial was examined. This would be expected to have the characteristic of an exponential reduction in number of errors, which were most trials with a low number of errors, fewer with medium number of errors and the least trials with high errors.

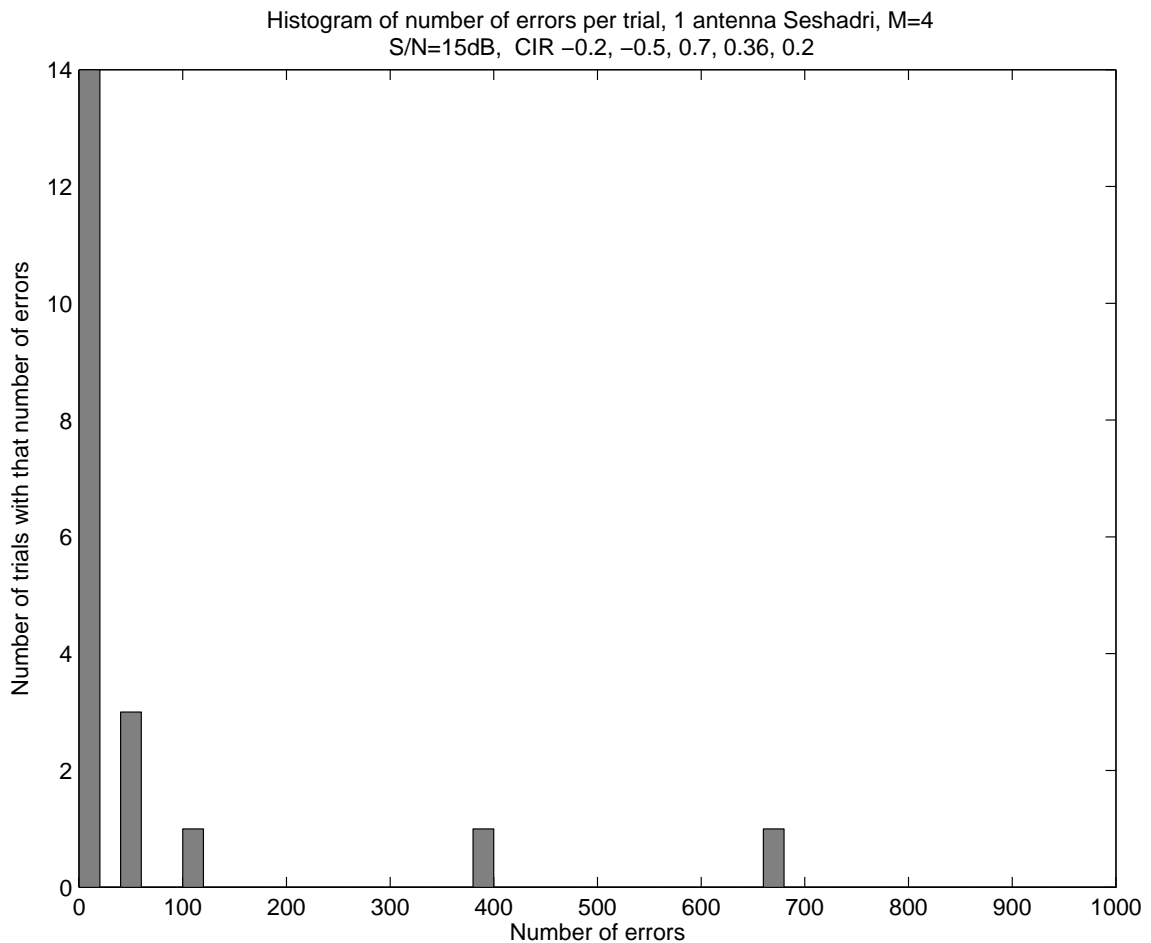


Figure 3.5-2 Example of the distribution of number of errors in 20 trials.

The simulation was set up as in Section 2.1.4 but S/N was fixed at 15 dB, only one CIR was used and 20 trials were done. A histogram was plotted with the number of errors returned that were divided into bands of 20 errors wide. Figure 3.5-2 showed the results that there were indeed most trials with low errors between zero and 20, three trials with between 40 and 60 errors, and one trial with between 100 and 120 errors, these

would have fitted the exponential characteristic but there were also two wild results with much bigger errors. These results could be explained by the slippage effect at work. Since it was actually the correct trellis used it may have taken a lot of samples for the undelayed trellis and CIR to get a better accumulated metric again.

The MLSE algorithm should have converged after 5 to 10 times the order of the CIR this should track one CIR not both to avoid this slippage. However, unlike the conventional VA, every trellis stored had its own CIR estimate; those trellises which were slipped, had CIR estimates which were offset in time as shown in Figure 3.5-1. The decision to keep a trellis was taken state by state, depending on the accumulated metric and this metric depended on the error between the received sample and the expected signal estimated from the CIR for that state. The slipped and non-slipped trellises would be in different states. So they would not be directly compared until the states were the same which occurred when the data sequence had a string of ones or minus ones. It appeared that it was possible for the combination of noise on the received sample and mis-adjustment of the CIR estimate from the LMS algorithm on the expected signal to allow the slipped trellises to survive. In general it was not possible to say if a trellis with delay δ samples was correct and that trellis with delay $\delta + 1$ was wrong. Error detection in the simulation took the data output sequence and found the delay which matched most closely the input data sequence as described in Section 2.1.4, so it did not matter if the data sequence was delayed by δ or $\delta + 1$. The problem was that the detection of data was done by using the trellis with the minimum accumulated metric, presumably the one with the best match to the best CIR estimate, but when two trellises had survived the data may be taken from either as they must have been giving about the same accumulated metric

for them both to survive. This switching from slipped to non-slipped was what causes the errors at the detector output.

The metrics that were accumulated were the squared errors between the received signal and the estimation of the next sample. When the estimated CIR order was the same as the true CIR order, $error_i = r_i - \hat{CIR}(state_i)$, where r_i was the received sample, \hat{CIR} was the estimated CIR, $\hat{CIR}(state_i)$ was the convolution operation and i was the sample index. For the correct data sequence $state_i = dataIn_i$ the error could be expressed as,

$$\begin{aligned} error_i &= \{CIR(dataIn_i) + noise_i\} - CIR(dataIn_i) + MCIR(dataIn_i), \\ error_i &= \{noise_i\} - MCIR(dataIn_i), \end{aligned} \quad (3.5.1)$$

where $dataIn$ was the transmitted sequence, CIR was the true CIR, $MCIR$ was the mis-adjustment of the CIR estimate and $noise_i$ was the sample of the noise. For the case of a slipped sequence the received sample was the same but the $dataIn$ and its estimated CIR coefficients were offset in time,

$$\begin{aligned} errorSlip_i &= \{CIR(dataIn_i) + noise_i\} - CIRslip(dataIn_{i-\delta}) + MCIRslip(dataIn_{i-\delta}) \\ errorSlip_i &= [CIR(dataIn_i) - CIRslip(dataIn_{i-\delta})] + \{noise_i\} - MCIRslip(dataIn_{i-\delta}) \end{aligned} \quad (3.5.2)$$

where δ was the offset in time that was a positive or negative integer, $CIRslip$ was the estimated CIR corresponding to the offset data sequence, and its corresponding mis-adjustment was $MCIRslip$. If these errors were the same some insight can be gained, since the true CIR and data was used for $error_i$ the errors are the best that could be expected;

$$\begin{aligned}
error_i &= errorSlip_i \\
noise_i - MCIR(dataIn_i) &= \\
CIR(dataIn_i) - CIRslip(dataIn_{i-\delta}) + noise_i - MCIRslip(dataIn_{i-\delta}) &\Rightarrow \\
CIR(dataIn_i) + MCIR(dataIn_i) &= CIRslip(dataIn_{i-\delta}) + MCIRslip(dataIn_{i-\delta}). \quad (3.5.3)
\end{aligned}$$

This meant that when the estimate from the ‘correct data’ trellis equalled the estimate from the slipped data trellis the errors will be the same, which was to be expected. However it did not specify that the estimates \hat{CIR} and $CIRslip$ alone gave the equality but the mis-adjustment of both must be taken into account.

From the theory of the LMS algorithm the mean squared error at any sample n was $J(n) = \text{trace}(RK(i)) + J_{\min}$, made of a transient part $\text{trace}(RK(i))$ from the LMS implementation plus constant J_{\min} the minimum mean squared error from the Weiner solution, [Hay96].

The part from the LMS implementation $\text{trace}(RK(i))$, where R was the correlation matrix of the received signal and $K(i)$ was the weight-error correlation matrix which could be found using some numerical trials. $K(i)$ was found from

$$K(i+1) = (I - \mu R)K(i)(I - \mu R) + \mu^2 J_{\min} R. \quad (3.5.4)$$

$$J_{\min} = E \left[|e_0(n)|^2 \right], \quad (3.5.5) \text{ and}$$

$$J_{ex}(\infty) = J_{\min} \sum_{i=1}^M \frac{\mu \lambda_i}{2 + \mu \lambda_i}, \quad (3.5.6)$$

the excess mean square error was the final value of the $\text{trace}(RK(i))$ term where $i = \infty$.

The minimum mean squared error could be written as,

$$J_{\min} = \sigma_d^2 - p^H R^{-1} p, \quad (3.5.7)$$

where σ_d^2 was the variance of the desired signal, p was the cross-correlation between the input to the estimated CIR and the desired signal, and R was the correlation matrix of the input to the estimated CIR. Considering an example of the case with no delay then with the true CIR = [-0.2 -0.5 0.7 0.36 0.2], S/N of 10 dB and including the transmit and receive filters the σ_d^2 was 0.29. The results were shown in Figure 3.5-3 along with the case with a delay of 1. From the complex baseband segment of the simulation in Section 2.1.4 the received signal was taken and R found from the inverse Fourier transform of the power spectral density of the received signal.

$$R = \text{Toeplitz}\left(N\Re\left(F^{-1}\left(\left(F(r)/N\right)\left(F(r)/N\right)^*\right)\right)\right), \quad (3.5.8)$$

where $\text{Toeplitz}(\cdot)$ meant the operation of generating a Toeplitz matrix from a vector (\cdot), $\Re(\cdot)$ was the operation of finding the real part and $F(\cdot)$ the discrete Fourier transform implemented by the fast Fourier transform method with $F^{-1}(\cdot)$ being it's inverse. To find the results for the slipped case the desired signal variance was the same and R the correlation matrix of the input to the estimated CIR was the same as well but the data used to generate the p matrix was shifted by one.

The first CIR had a slipped error that comes much closer to the no slip error indicating that it would be easier to mistake the slipped data sequence when working with the first CIR, which was illustrated by the worse BER performance in Figure 3.2-1. From the histogram in Figure 3.5-2 the number of errors was found to extend up to about 675 errors this would be past the transient in the LMS learning process and the possibility of slippage would depend on the final values of the mean squared error.

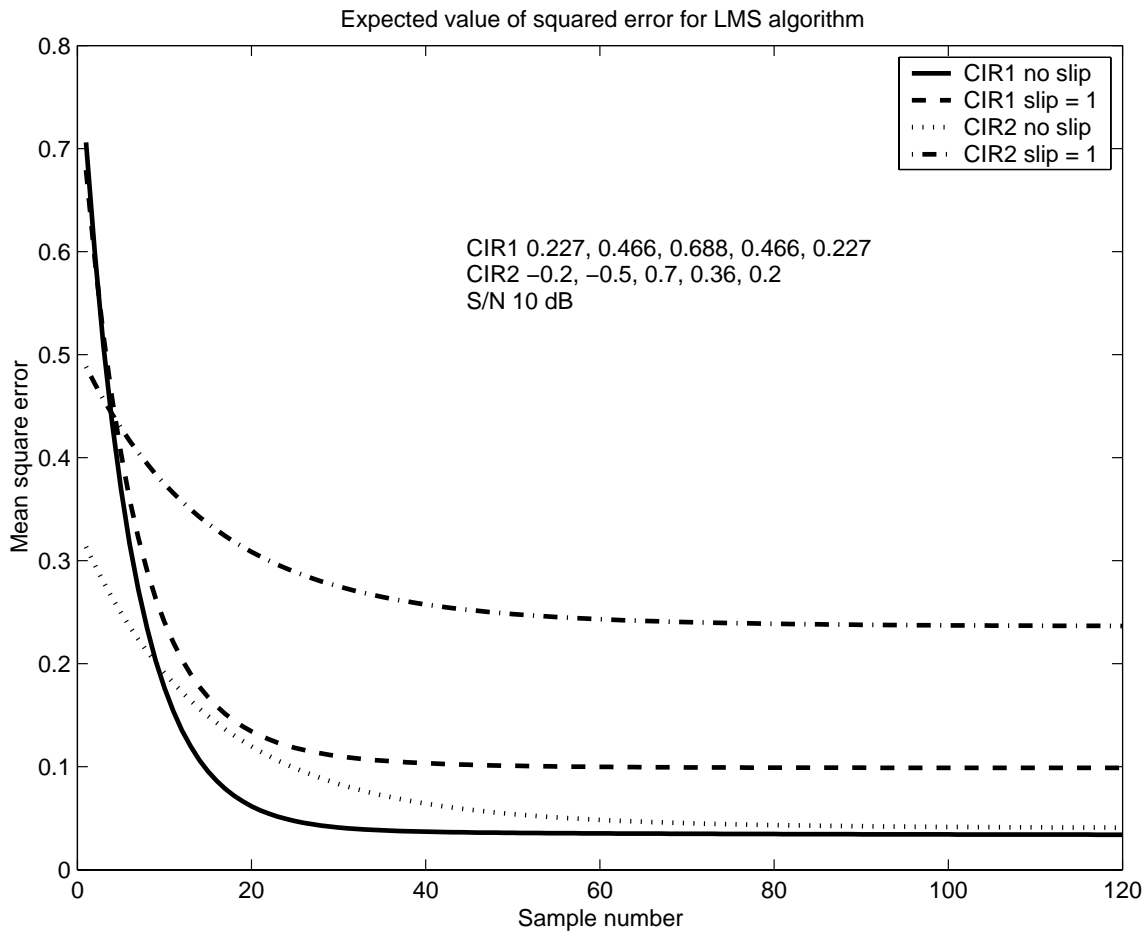


Figure 3.5-3 Evolution of expected value of error for two CIRs showing difference between no slip and slip of one sample delay.

Figure 3.5-4 showed how these vary with S/N ratio, again the difference in error for the first CIR was much less indicating it was much more likely to suffer slippage over all S/N ratios. This was generated by solving for J_{min} and $J_{ex}(\infty)$ over the usual range of S/N values using the complex baseband model of the simulation described in Section 2.1.4.

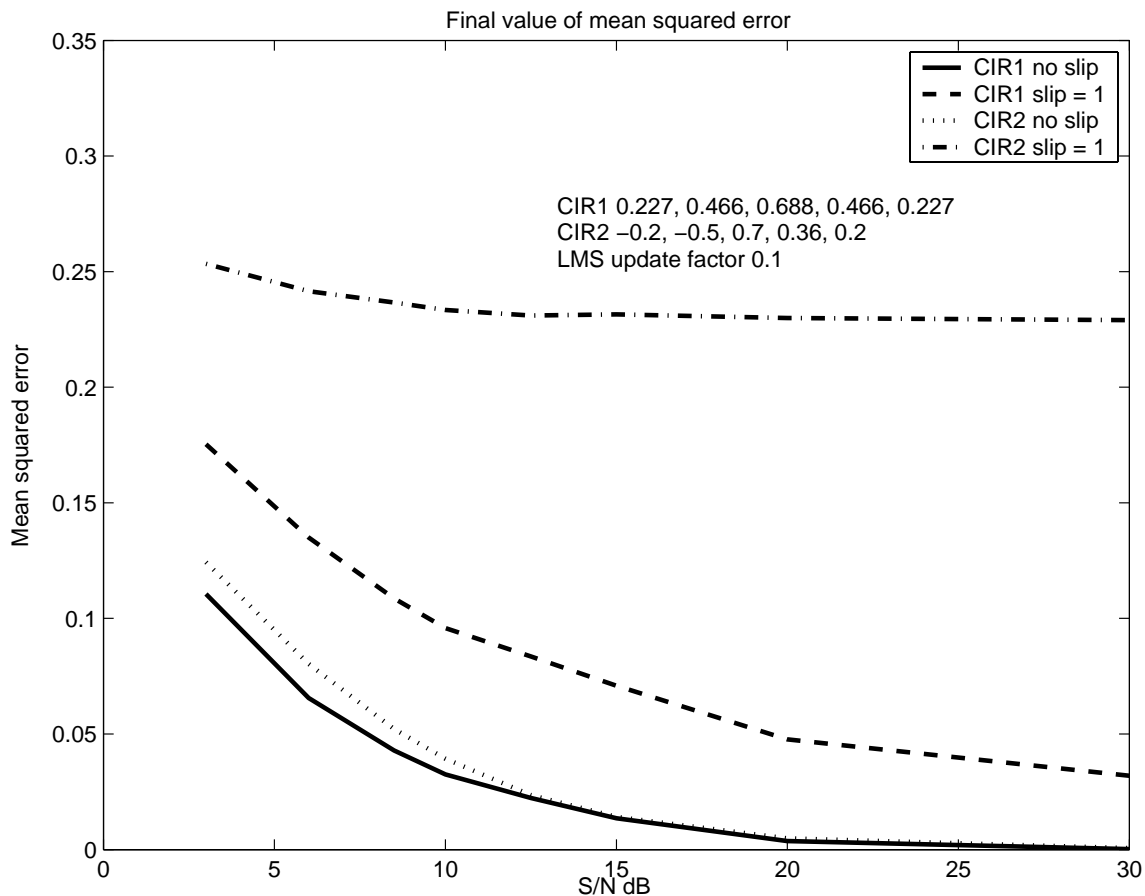


Figure 3.5-4 Final mean squared error from LMS algorithm with two CIRs using data with no slip and slip of one sample delay.

To demonstrate this occurred in the simulation two trellises were used to generate Figure 3.5-5, the first trellis was the non-slip version of the transmitted data and the second the trellis with one sample delay. The simulation allowed the LMS algorithm to learn each CIR and the centre and right hand plots showed where the accumulated metric was less for the slipped trellis compared to the non-slipped one. As described earlier in this section not all trials had slip errors, the simulation was run until this result was found.

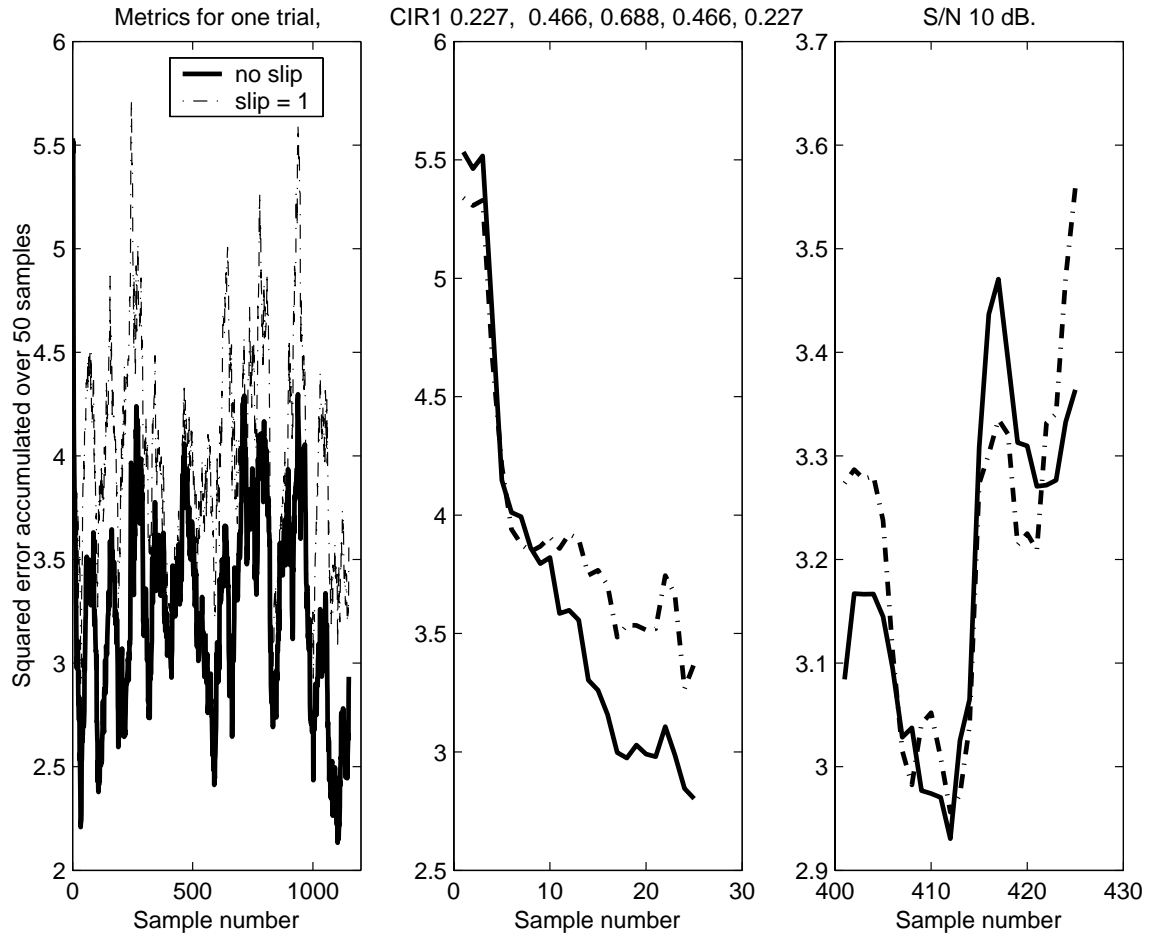


Figure 3.5-5 Accumulated metric from one trial showing two slippages at the start up and later in the trial.

Another way of looking at this was to compare the operation of estimating the next sample. In the case of the sequence with no delay the data and CIR were lined up as:-

$$\begin{bmatrix} data1 & data2 & data3 & data4 & data5 \\ CIR1 & CIR2 & CIR3 & CIR4 & CIR5 \end{bmatrix},$$

While the delayed data case had led the LMS algorithm to generate the same coefficients corresponding to the four data from the un-delayed case but the CIR0 coefficient corresponding to the older data tended to zero to reduce the error.

$$\begin{bmatrix} data0 & data1 & data2 & data3 & data4 \\ CIR0 & CIR1 & CIR2 & CIR3 & CIR4 \end{bmatrix}$$

The difference between the estimates of the next sample was in the difference between the estimate CIR0 and CIR5. During start up when the CIR was being learnt the both CIR0 and CIR5 may have been equal.

If the S/N ratio was such that the noise was larger than the effect of CIR0 and CIR5 their values did not influence the error between the next sample estimates.

Serious errors per trial occurred when the DSA could choose between two or more trellises; the worst case was when the two trellises were those with slip delay +1 and -1 sample periods. It was so bad because CIR1 and CIR2 both had the first and last coefficients the same magnitude, which means the metrics from slip delay +1 and -1 would be almost equal. This was illustrated by changing the last coefficients of CIR1 and CIR2 as shown in Figure 3.5-6, other wise the simulation was set up as in Section 2.1.4 and the results from Figure 3.2-1 put in for comparison.

For the equal first and last coefficients, as the S/N ratio was increased this did not improve the BER as the accuracy of the slipped CIR estimates improved keeping the two accumulated metrics almost the same. This came from the loss of the trellis with zero delay, which may have occurred during start up as the first decision to discard trellises was taken after only $O + \log_2(2M)$ samples as described in Section 3.2. The correct CIR was not regenerated because those trellises with slip delay have propagated to occupy all the stored trellises, CIR estimates and metrics.

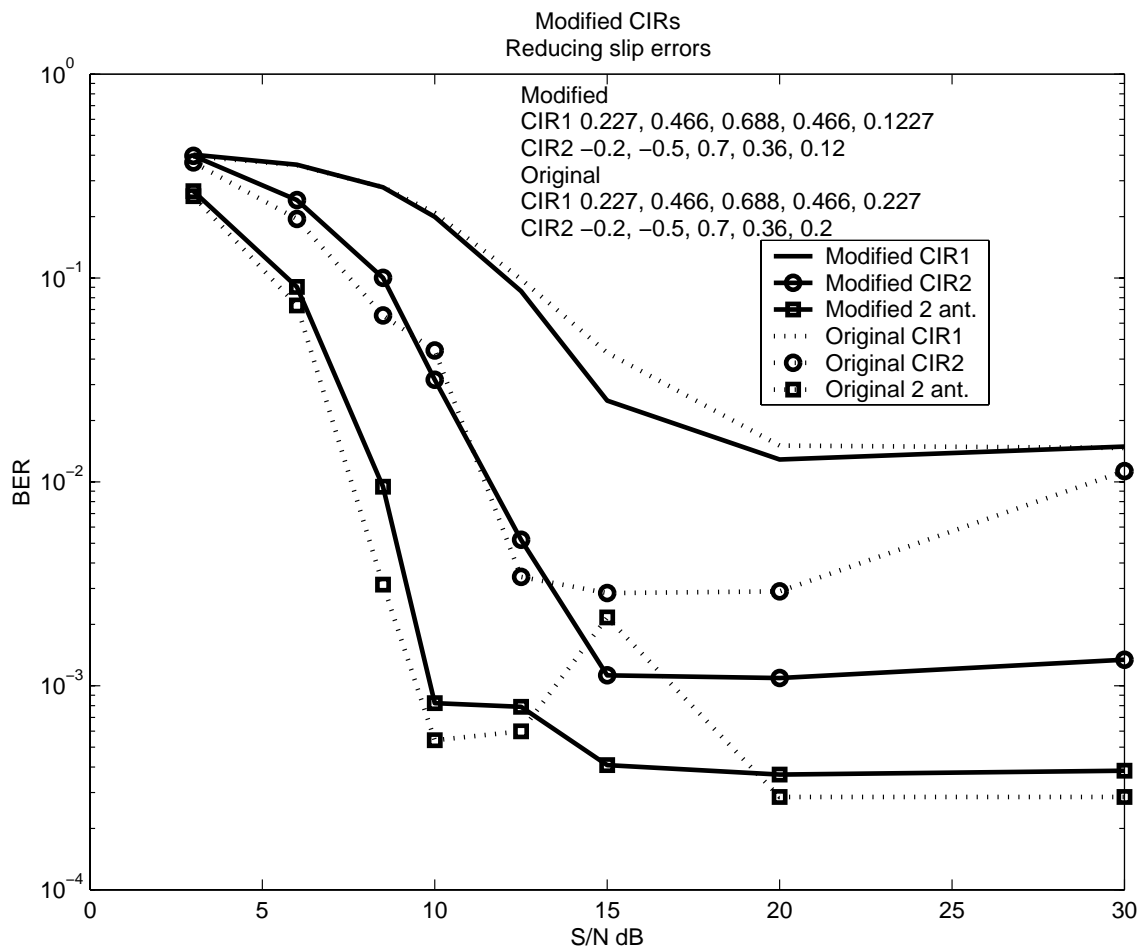


Figure 3.5-6 CIRs without first and last coefficients equal.

It was observed to be particularly often the cause of errors using the two antenna diversity. By using two antenna diversity it appeared that both slipped versions were more likely to survive than using only one antenna, this was attributed to the link between the antennas being the metric used to choose the survivors. When linked together the CIR that had lower error at the beginning, whether the true or slipped one, made the metric lower for that trellis and so more likely to survive. This in turn ensured the other CIR estimate works on the correct or slipped trellis.

There appear to have been two conflicting requirements, first data rich enough to teach the LMS algorithm the CIR quickly and second strings of ones or minus ones to

get the selection algorithm to select either the correct or slipped trellis allowing only one to propagate. The length of the strings needed to be $O + 1$. As the estimated order was made higher this would have been more unlikely to occur during the LMS learning period.

This explained the bursts of errors when the correct order of CIR had been chosen and when the estimated order was greater than the true order. The other major source of errors was from the start up or learning stage, which would have been expected to have formed the ‘floor’ to the BER versus S/N plots.

With the application of diversity in Section 3.2 the BER performance was significantly better as seen by the lower floor of the BER, the possibility of slippage was reduced with diversity because the second signal path had to have a slippage at the same time as the first, since this was not the case it achieved a lower accumulated metric from both paths.

3.6 Comments on assumptions and sources of error

Both the simulations and derivation of the optimal combining of diversity antennas assumed the noise was uncorrelated. This would be true in practice in a number of scenarios. If the noise contribution from the receiver electronics before the sampler dominated the noise and interference. If the interference was dominant over the receiver generated noise and the interference was uncorrelated at each antenna, since the desired signal is assumed uncorrelated and there would be a number of interferers. Finally if the sample times were different at each antenna due to the operation of the symbol timing recovery, the noise samples would be uncorrelated. It therefore seemed a reasonable assumption to use.

One CIR could have been delayed more than the other, if delay was more than O sample periods the CIR for one channel would always produce major errors, however assuming coincidence of CIRs seems a realistic reflection of the practical positioning of antennas.

Using the trellis with the lowest accumulated metric as the data detector attempted to avoid the issue of confusing two or more surviving sequences from slipped versions of the trellis, by assuming the trellis with no slip was present and would have the lowest metric. Another way which was found more prone to errors was taking a majority decision from all the trellises.

The error detector found the offset which best matches the transmitted data over the whole trial, this masked the effect of slippage where no change in the delay took place; if the same trellis with slip was used for the whole trial zero errors could be produced.

The number of trials was to be controlled by a number of errors target of 100, but any slippage introduced a burst of the order of 100 and so would stop the simulation, therefore a fixed number of trials was used to give a fair chance at each S/N point.

In the simulations the DSA started when the signal had been present for 36 samples, in practice the receiver would need time to perform carrier synchronization etc see Section 2.1. There would also be some framing somewhere in the communication system so the first samples to be received after recovering from a deep fade or starting the receiver would probably not be the first symbols of a frame, and these would be discarded during later processing. The error detector worked with the all the data received to show the fast operation, which was a desirable feature, that was possible to

achieve with this DSA. So at start up the CIR estimates and metrics were set to be zero, however if the DSA was started before a signal was present the CIR estimates were small random values as were the metrics this would have increased the possibility of losing the correct trellis, because the random CIR for the correct trellis may produce worse estimates of the received signal than another trellis and so be discarded. It was assumed that the synchronization discussed in Section 2.1 was able provide a trigger to start the DSA.

Synchronization seemed to be the most severe assumption, as the eye diagrams in appendix E indicated; Meyr et al. [MeMoFe98] detail optimal joint detection and synchronization as suggested by Raheli et al. [RaPoTz95]. It was common in the literature to find synchronization assumed and the technique in this thesis should be compatible with the extension suggested in Section 4.2.1. However Meyr et al. [MeMoFe98] made the observation that it was possible to make maximum likelihood detection by maximizing $P(r|d)$ without any synchronization, using fractionally spaced sampling.

Similarly to synchronization the automatic level control (ALC) was required to get the magnitudes of the metrics at both antennas the same and avoid weighting one more than the other. This annulled one of the advantages of Seshadri's single antenna system that it had some built in level control. To get around this in practice normalization could be used and the received power measured during synchronization in the digital domain or the classic ALC loop could be linked to the analog part of the RX between the antenna and sampler. An analog implementation may have been necessary to allow the sampler to operate at its optimum dynamic range.

Chapter 4 Conclusions and Future Improvements

4.1 Performance

4.1.1 Improvement by the optimal combining of a second antenna.

When the true order of the CIRs was used and they were equal, the addition of the second antenna improved the performance better than either of the two antennas taken alone. In Figure 3.2-1 for a BER of 5×10^{-3} a 4 dB improvement over the better channel was achieved. Diversity gain above the gain from increased received power at the second antenna was difficult to define due to the different performance of the CIRs at each antenna and the presence of the slip and start-up errors. In the case that the CIR of the second antenna had a different order to the first CIR the diversity combination with the estimated CIR order equal to either of the true CIR orders equalled or exceeded the single antenna performance for that CIR. To reduce the number of computations it would have been convenient to be able to use the estimated CIR order less than the true one and achieve good performance, this appears to be possible in some cases but not all, these cases may be uncommon see Section 4.2.1 for further work.

With a wrong order of estimated CIR the DSA performance may even be slightly worse than a single antenna, and that performance was about two orders of magnitude worse than using the true CIR order. When the order of the estimated CIR was greater than the true order, the DSA succeeded in finding the true CIR but errors were introduced by allowing the slipped CIR and trellis to exist.

4.1.2 Operation during start up.

Errors were not evenly spread over the trials with the two antenna diversity. Rather than that most trials had zero or less than ten errors, while one trial had of the order of two hundred errors, and that high error would dominate the BER producing peaks even though the S/N ratio was high. Slippage was the cause of these high errors, due to the non-convergence of the trellises into one. This effect could be reduced either by diversity or by increasing M . It was due to the survival of two or more trellises since the beginning of the DSA. At the very beginning of the DSA an exhaustive search was made whilst the trellis filled to $O + \log_2(2M)$ samples long. During the exhaustive search period all possible trellises were present, including the correct and slipped versions of it, and then trellises started to be discarded. This is especially serious if the trellis with no slip delay is lost but two of the survivors are those with slip +1 and -1, because the CIRs chosen for simulation both had lost a coefficient with the same magnitude which contributed the same error to the metric. By using two antenna diversity it appeared that both slipped versions were more likely to survive than using only one antenna, this was attributed to the link between the antennas being the metric used to chose the survivors. When linked together the CIR that had lower error at the beginning, see Section 3.5, whether the true or slipped one, made the metric lower for that trellis and so more likely to survive. There appeared to be two conflicting requirements neither of which are under the control of the receiver, the first was data rich enough to teach the LMS algorithm the CIR quickly and the second was strings of ones or minus ones to get the selection algorithm to select either the correct or slipped trellis allowing only one to propagate.

4.1.3 Performance after convergence of M trellises.

As shown in Section 3.4 the M trellises kept per state gradually converged to be the same. If the DSA was left running and the signal suffered fading the performance of the M trellises kept per state would have been lost unless the trellises could have been reset in some way to introduce the extra paths into the states. In practice the longer the DSA was running the more likely the CIR would be to change and more need to be able to track it. This seemed to be a serious difficulty with the DSA.

4.2 Suggestions for Future Improvements

4.2.1 Control order of CIR estimate to avoid “slippage”

An ad hoc solution would be to make a detector of slippage. However it may be better to look at the underlying problem and investigate use of some form of “tap-centering” as suggested by Foschini [Fos85] or maximizing the S/N ratio.

The possibility of having a CIR that can be well modelled by a lower order, from Section 3.3, would allow a lower number of computations. This could be checked while some of the synchronization required is being achieved, by examining the correlation matrix of the received signal. This could also be used to optimize the LMS update step, by finding the eigenvalues of the correlation matrix, each antenna should have optimized its own μ value to match the CIR it was suffering.

Those four CIRs used in the simulations were only a selection from the whole range of possibilities and further work would be required to generalize conclusions.

As shown in Section 3.4, there was a trade off between M and diversity, to control the number of slip errors at high S/N more antenna diversity with four or more

antennas may avoid having to increase M . Using M has been shown to only work at the beginning of the DSA, it would not be elegant to have to reset the M trellises to regain this performance during fading.

Fading is a common feature of radio channels, it is often characterised by a Rayleigh distribution. By including a Rayleigh fading model the consequences of the convergence of the M trellises could be explored.

To enable a practical receiver the combination of optimal joint detection and synchronization detailed by Meyr et al. [MeMoFe98] may be incorporated. Or the fractional spaced sampler technique mentioned in Section 2.1 could be employed.

4.2.2 Multi-user version for CDMA use

As shown in Appendix G the CIRs for multiple users could be extracted by making a new definition of the error and CIR update. Since the error is not assigned to individual CIRs for this extraction, the maximum likelihood algorithm for each user would require the development of another stage to remove the contributions to each CIR from the others, which should not be too difficult. The trellises would be made up of each possible chip sequence which was fixed in some known way, so a way of defining the set chip patterns needs to be identified to assemble the trellises.

References

- [1xEVDO] “cdma2000 High Rate Packet Data Air Interface Specification, C.S0024,” Technical Specification Group C of the Third Generation Partnership Project 2 (3GPP2). September 12, 2000.
- [Bel86] S. Bellini, “Bussgang techniques for blind equalization,” in Proc. *IEEE Global Telecommunications Conf.*, (Houston, Texas), pp. 1634–1640, December 1-4, 1986.
- [BiPrSh98] E. Biglieri, J. Proakis and S. Shamai, “Fading Channels: Information-Theoretic and Communications Aspects,” *IEEE Trans. on Information Theory*, vol. 44, no. 6, October 1998.
- [Bus52] J.J. Bussgang, “Cross Correlation Functions of Amplitude-Distorted Gaussian Signals,” Tech. Rep. 216, MIT Research Laboratory of Electronics, Cambridge, Mass. 1952.
- [ChHo01] X. Chen and P.A. Hoeher, “Blind Equalization with Iterative Joint Channel and Data Estimation for Wireless DPSK Systems,” *GlobeCom 2001 ASP05-02*, October 23, 2001.
- [ChLu99] S. Chen and B.L. Luk, “Adaptive simulated annealing for optimization in signal processing applications,” *EURASIP Signal Processing Journal*, vol. 79 , no. 1, November 1999 , p 117-128
- [ChPo96] K. Chugg and A. Polydoros, “MLSE for an unknown channel, Part I: Optimality considerations,” *IEEE Trans. Commun.*, vol. 44, no. 7, pp. 836–846, July 1996; “Part II: Tracking performance,” August 1996.
- [DuHe85] A. Duel and C. Heegard, "Delayed decision feedback sequence estimation," *Conf. Rec. 23rd Conference on Communications, Control and Computers*, pp. 878-887, October, 1985.
- [EyQu88] M.V. Eyuboğlu and S.U.H. Qureshi, “Reduced-state sequence estimation with set partition and decision feedback,” *IEEE Trans. Commun.*, vol. 36, no. 1, pp. 13–20, January 1988.
- [Fos85] G.J. Foschini, “Equalization without altering or detecting data,” *Bell Syst. Tech. J.*, vol. 64, no. 10, pp. 1885-1911, October 1985.
- [GeWi81] R.D. Gitlin and S.B. Weinstein, “Fractionally-spaced equalization: an improved digital transversal filter,” *Bell Syst. Tech. J.*, vol. 60, no. 2, pp. 275-296, February 1981

- [God80] D.N. Godard, "Self-recovering equalization and carrier tracking in two-dimensional data communication systems," *IEEE Trans. Commun.*, vol. 28, no. 11, pp. 1867–1875, November 1980.
- [HaNi91] D. Hatzinakos and C.L. Nikias, "Blind equalization using a tricepstrum-based algorithm," *IEEE Trans. Commun.*, vol. 39, no. 5, pp. 669–682, May 1991.
- [HaNi94] D. Hatzinakos and C.L. Nikias, "Blind equalization based on higher-order statistics (HOS)," in *Blind Deconvolution*, ed. S. Haykin, Prentice-Hall, Englewood Cliffs, N.J. 1994.
- [Hay96] S. Haykin, *Adaptive Filter Theory*, Englewood Cliffs, New Jersey 07632, USA, Prentice-Hall, Inc., 3rd ed., 1996.
- [HoJoLe01] S.C. Hong, J.S. Joo and Y.H. Lee, "Per-survivor processing sequence detection for DS/CDMA systems with pilot and traffic channels," *IEEE Comms. Letters* vol. 5, no. 8, August 2001.
- [HRPD0032] "Recommended Minimum Performance Standards for cdma2000 High Rate Packet Data Access Network," C.S0032, Technical Specification Group C of the Third Generation Partnership Project 2 (3GPP2), December 2001.
- [JeYe97] Y.J. Jeng and C.C. Yeh "Cluster based blind nonlinear channel estimation," *IEEE Trans. Signal Process.*, vol. 45, no. 5, pp. 1161-1172, May 1997.
- [Luc66] R.W. Lucky, "Techniques for adaptive equalization of digital communication systems," *Bell Syst. Tech. J.* vol. 45, no. 2, pp. 255-286, February 1966.
- [LuSaWe68] R.W. Lucky, J. Salz, and E.J. Weldon, *Principles of Data Communications*, New York: McGraw-Hill, 1968.
- [MeMoFe98] H. Meyr, M. Moeneclay, S. Fechtel, *Digital Communication Receivers*, New York: J. Wiley, 1998.
- [PrNi91] J.G. Proakis and C.L. Nikias, "Blind Equalization," *Adaptive Signal Processing, Proc. SPIE*, vol. 1565 December 1991.
- [Pro83] J.G. Proakis, *Digital Communications*, McGraw-Hill, New York, 1983.
- [RaPoTz95] R. Raheli, A. Polydoros, C.K. Tzou, "Per-Survivor Processing - A general approach to MLSE in uncertain environments," *IEEE Trans. Commun.*, vol. 43, nos. 2-4, pp. 354-364, February-April 1995.

- [Rap96] T.S. Rappaport, *Wireless Communications, Principles and Practice*, Prentice Hall Inc.. 1996.
- [Sat75] Y. Sato, "A method of self-recovering equalization for multilevel amplitude-modulation systems," *IEEE Trans. Commun.*, vol. 23, no. 6, pp. 679–682, June 1975.
- [ScPeSe99] R. Schlagenhauser, B.R. Petersen, A.B.Sesay "Delayed-Decision-Feedback Equalization for Multiuser Systems," *Conf. Proc. of Wireless 99*, Calgary, Alberta, Canada, vol. 1, pp. 71-84, July 12-14, 1999.
- [SeAn88] N. Seshadri and J.B. Anderson, "Decoding of severely filtered modulation codes using the M-algorithm," submitted to *IEEE ICC 88*, (Philadelphia, PA, USA), June, 1988.
- [Ses94] N. Seshadri, "Joint data and channel estimation using blind trellis search techniques," *IEEE Trans. Commun.*, vol. 42, nos. 2-4, pp. 1000–1011, February/March/April 1994.
- [Sim90] S.J. Simmons, "Breadth-first trellis decoding with adaptive effort," *IEEE Trans. Commun.*, vol. 38, no.1, pp. 3–12, January 1990.
- [ToXuKa91] L. Tong, G. Xu, and T. Kailath, "A new approach to blind identification and equalization of multipath channel," in *Proceedings of the 25th Annual Asilomar Conference on Signals, Systems, and Computers*, Pacific Grove, vol. 2, pp. 856–860, November 1991.
- [ToXuKa94] L. Tong, G. Xu, and T. Kailath, "Blind channel identification based on second order statistics: A time-domain approach," *IEEE Trans. Inform. Theory*, vol. 40, no. 2, pp. 340-349, March 1994.
- [VeTaPa97] A.J. van der Veen, S. Talwar, and A. Paulraj, "A Subspace Approach to Blind Space-Time Signal Processing for Wireless Communication Systems," *IEEE Trans. Signal Process.*, vol. 45, no. 1, pp. 173-190, January 1997.
- [WoJa65] J.M. Wozencraft and I.M. Jacobs, *Principles of Communication Engineering*. New York, NY, USA: John Wiley & Sons Inc., 1965.
- [ZePrEy92] E. Zervas, J. Proakis and V. Eyuboğlu, "A 'quantized' channel approach to blind equalization," in *Conf. Rec. IEEE ICC 92*, vol. 3, (Chicago, IL, USA), pp. 1539-1543, June 14-18, 1992.

Appendixes

A. Transmit and receive filter frequency response

This was sampled at twice the symbol rate.

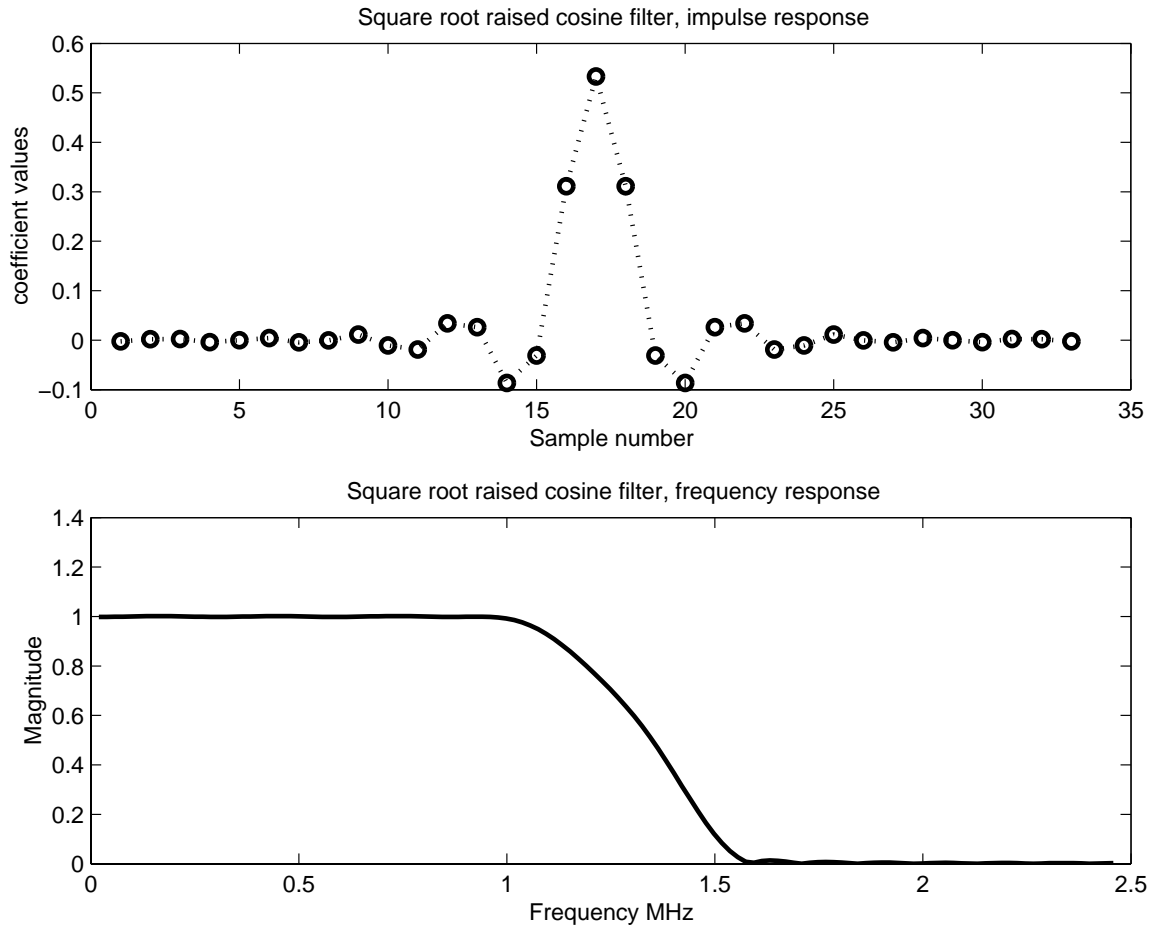


Figure A.1 Transmit and receive filter coefficients and frequency response.

To confine the transmitted signal in the frequency spectrum a filter was applied to the data waveform. Further to avoid inter-symbol interference from the filtering identical square root raised cosine shapes was chosen at the TX and RX. The transfer function was defined by Rappaport [Rap96],

$$H(f) = \begin{cases} 1 & 0 \leq |f| \leq (1-\alpha)/2T_s \\ \sqrt{\frac{1}{2} \left[1 + \cos \left(\frac{\pi(2T_s |f| - 1 + \alpha)}{2\alpha} \right) \right]} & (1-\alpha)/2T_s < |f| \leq (1+\alpha)/2T_s \\ 0 & |f| > (1+\alpha)/2T_s \end{cases} \quad (A.1)$$

where the roll off factor α was defined in terms of percentage by the excess bandwidth EXBW. $\text{EXBW \%} = \alpha/100$. 25 % excess bandwidth was used for all the simulations as a trade off between spectral restriction and the number of significant coefficients. Having the frequency response gave the impulse response by the inverse Fourier transform. The impulse response was truncated to 33 points. The frequency response shown was generated by the fast Fourier transform of the 33 point impulse response padded with zeros to achieve a smooth curve.

B. Algorithm performance with reference CIR

To check the operation of the simulation a reference CIR = [1] was used for both the one antenna and DSA.

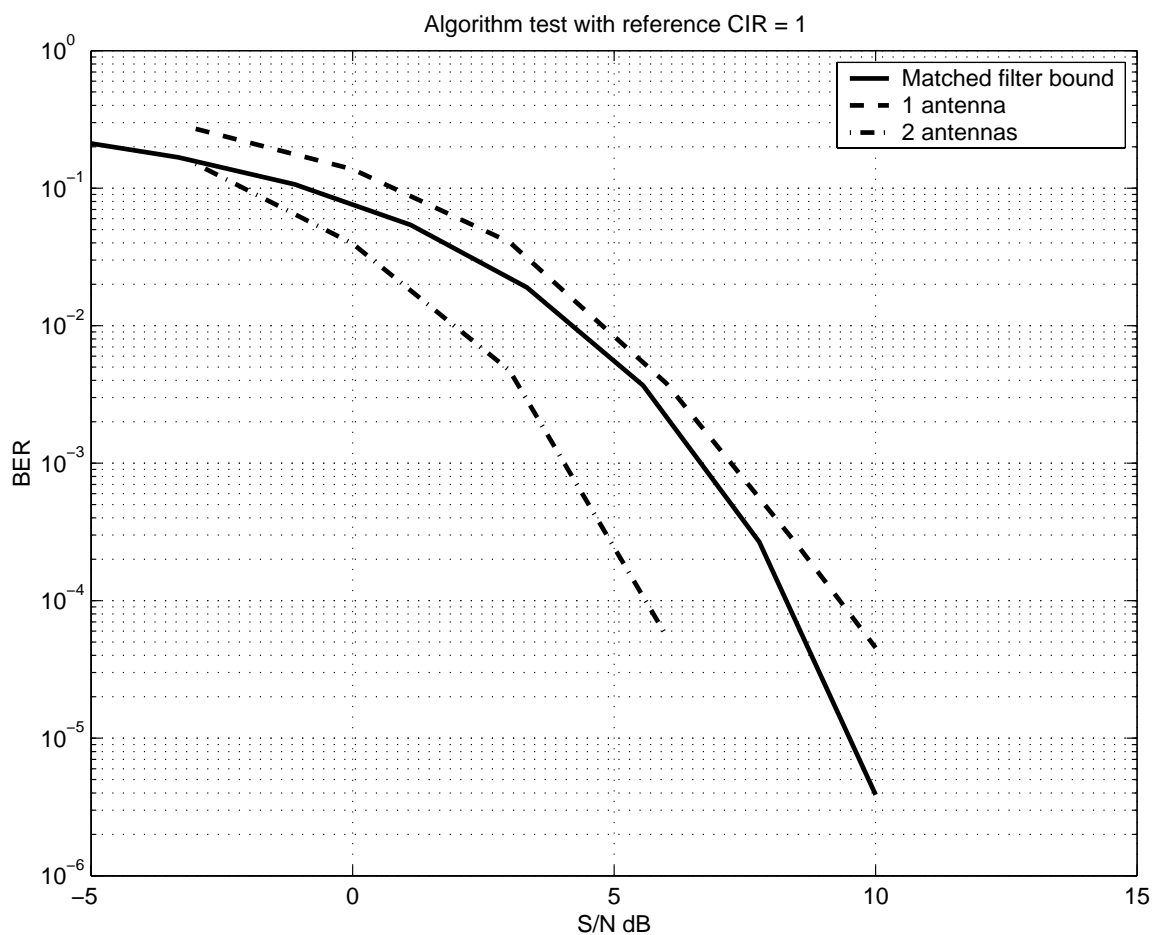


Figure B-1 Results for reference CIR = 1, using single and diversity antennas.

This simulation was set up following the steps of Section 2.1.4 but O was set to one, and the same CIR was used for both antenna channels so only one single antenna curve was used to compare to the diversity channel. Considering the single antenna trace in Figure B-1, it would have been expected to fall on top of the matched filter bound. Since my DSA used differential data it gave two errors for one error in the raw detected

data. The next Figure B-2 shows the single antenna error rate above divided by two. Considering the diversity results it appeared to have better than matched filter performance, this was due to the combining of the metrics taking the effect of exactly the same received data from the transmitter over two paths of CIR = 1 but different noise, this effectively increased the S/N by 3 dB as expected, see Section 3.2. In Figure B-2 the diversity antenna error rate was shifted to the right 3 dB and divided by two. Above 8 dB S/N the results diverge again as start up errors dominated.

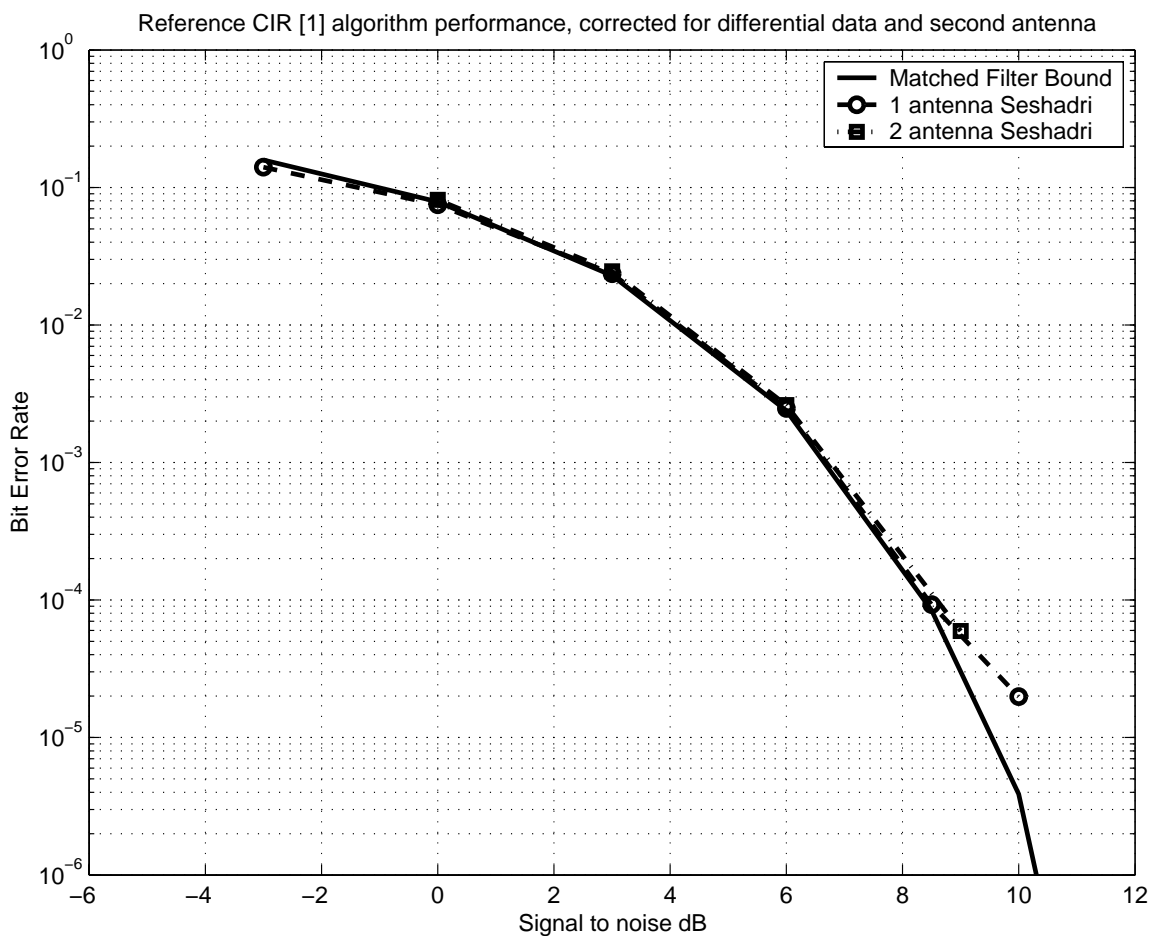


Figure B-2 Corrected reference BER performance for reference CIR.

C. More results

One variable was the length of the trellises kept until a data decision taken, which was the truncation of the MLSE. The simulation was set up as in Section 2.1.4 but instead of running the single antenna algorithm with each of the CIRs the DSA was run three times for each received sequence with N set to 25, 50 and 100. These results confirmed assumption that truncating the trellis after 100 samples was sufficient to find the best trellis.

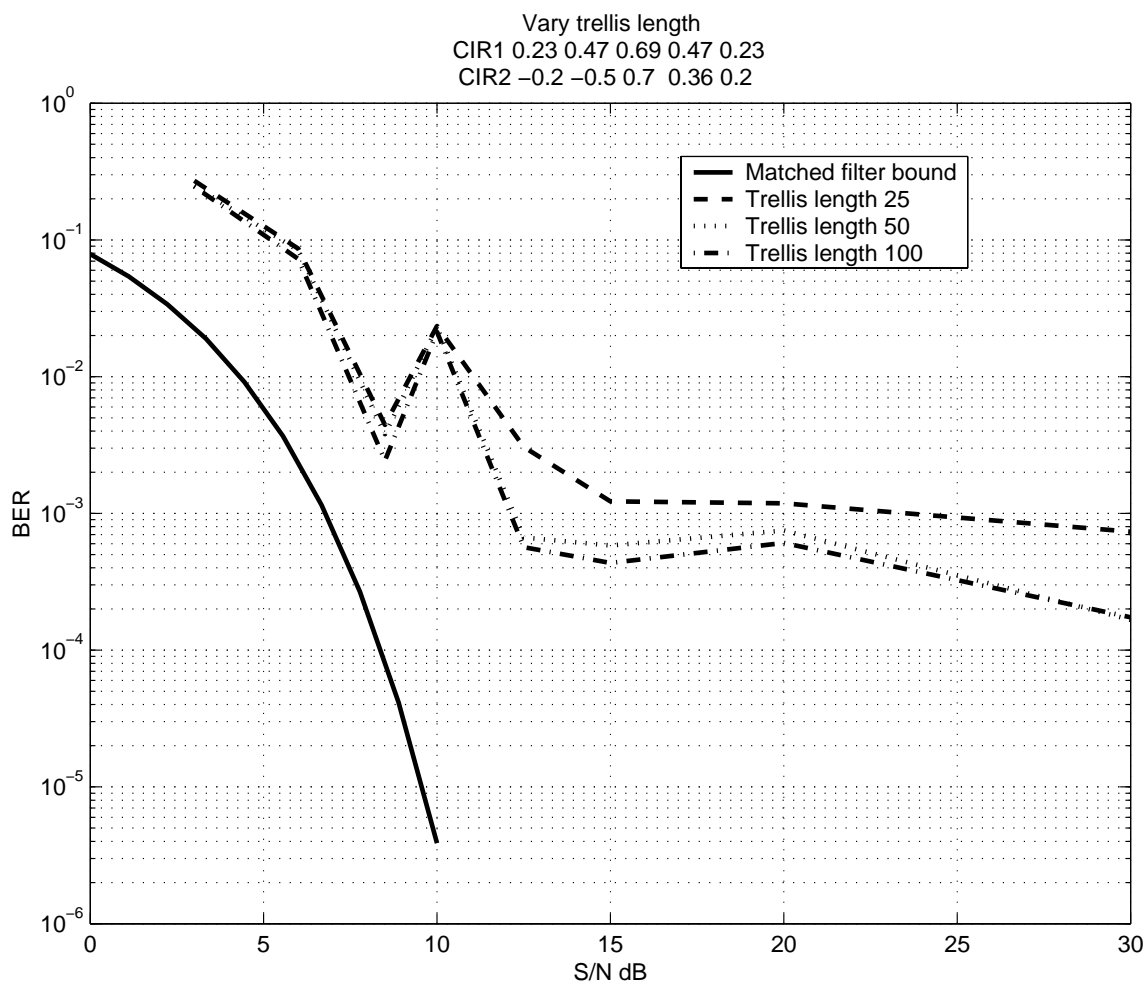


Figure C-1 Variation of trellis length.

The presence of two trials at 10 dB S/N with slip effects showed in all three lengths of trellis, which suggested that the propagation of two distinct trellises was difficult to stop. There was some marginal improvement with 20O and since the only cost was some extra memory that may be worth while.

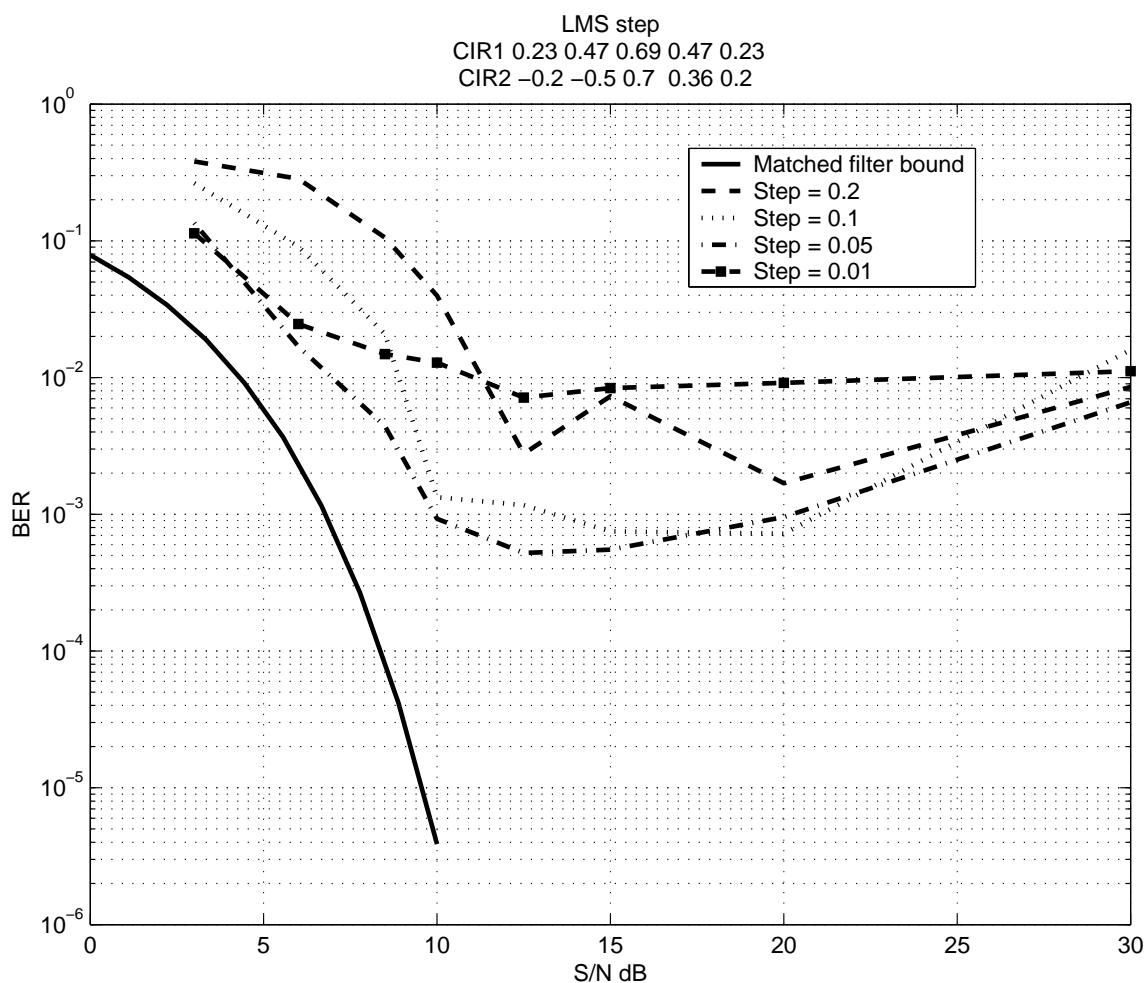


Figure C-2 Variation of μ in LMS algorithm for CIR updating for two antenna diversity.

Another variable was the LMS step, μ , for CIR updating, the simulation was set up as in the previous experiment but here N was fixed again at 50 and the DSA run four times with $\mu = 0.2, 0.1, 0.05,$ and 0.01 for each received sequence. The presence of

slip appeared in all trials as did the start up errors. With a smaller value of μ the errors were lower as would have been expected for a more accurate estimate of the CIR, but the BER floor at high S/N had an optimal value. This optimal value was where the trade off between slow convergence allowing two trellises to exist which lead to slip errors and the better prediction of received symbols minimized the overall BER. It appeared to between $\mu = 0.1$ and 0.05 was where the optimum lay for that experiment; see Section 4.2.1 for further work to optimize this. It appeared that the μ value had some control over the number of slip errors as the peak for $\mu = 0.2$ at 15 dB S/N which was due to one trial with 222 errors was not reflected in any of the other μ values that were offered the same received signal, but they did all have slip errors at 30 dB S/N.

For the performance after start up, that was after 100 samples until sample 1200 , which removed the effect of errors early in the CIR learning process. This experiment took the results from Figure 3.2-2 and subtracted them from those in Figure 3.2-1 leaving the after start up errors. Although this appeared to show the performance of the DSA approached the matched filter bound, there were two factors to be taken into account, first the DSA performance should have achieved 3 dB improvement due to the extra signal and second in practice by sample 1200 the channel would have started to encounter fading. In the CIR2 trace the effect of the slip errors for S/N 30 dB could still be seen see Section 3.5.

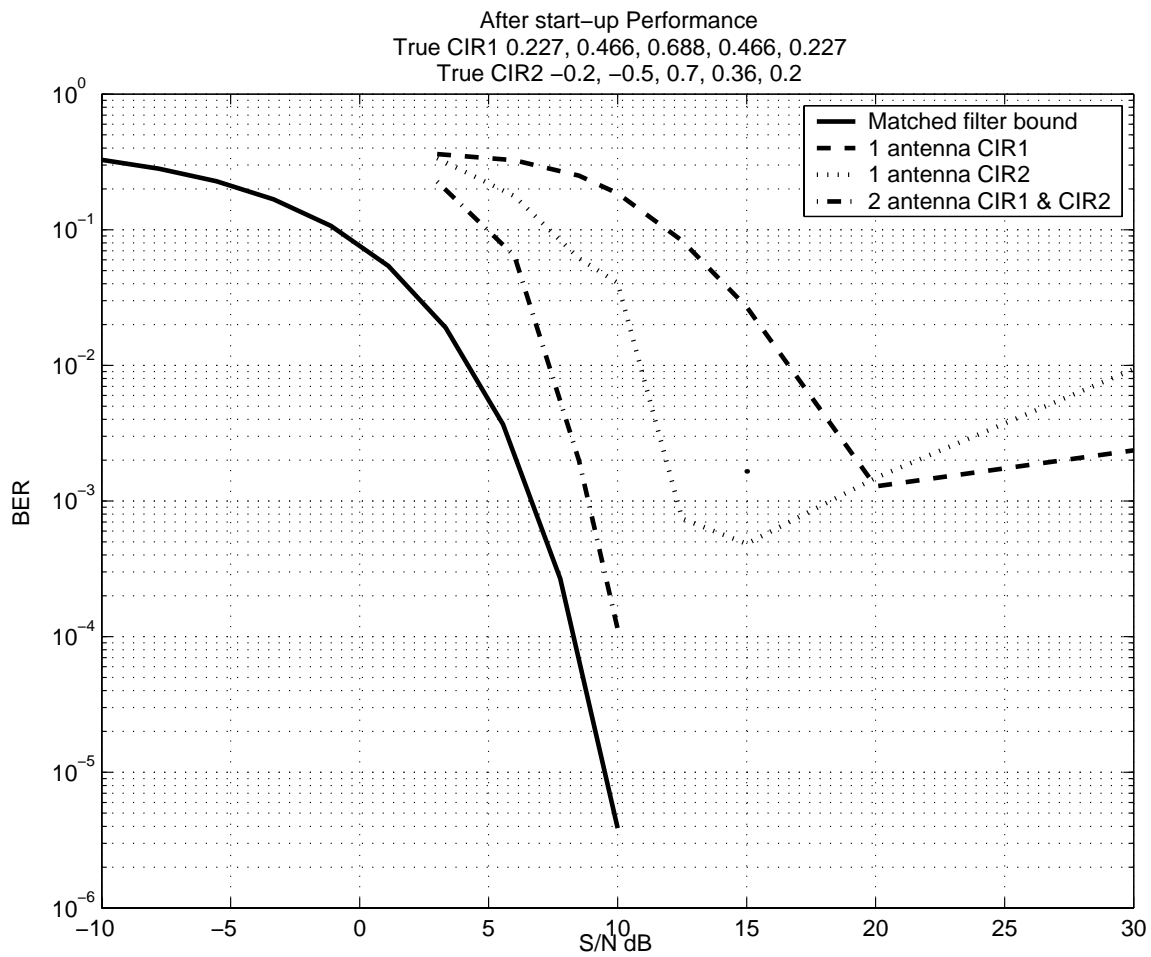


Figure C-3 Performance with start up errors removed.

D. Number of complex calculations per sample

Where A was the number of antennas, but finding the differential data output or doing the sorting were not included in these numbers.

Task	Multiplications	Additions
Error for each state and M trellises per state	$AO2M2^O$	$A(O+1)2M2^O$
Metrics	$A2M2^O$	$2M2^O$
Accumulate metric	zero	$2M2^O2^*$
CIR update	$A2O2M2^O$	$A(O+1)2M2^O$
Total	$A2M2^O(3O+1)$	$2M2^O(2A(O+1) + 3)$

* The newest column of metrics would be added and the oldest subtracted.

Table D-1 Number of complex calculations required per sample.

Taking M = 4, O = 5 and A = 2 the number of complex calculations were:-

Task	Multiplications	Additions
Error for each state and M trellises per state	$2.5.2.4.2^5 = 2560$	$2(5+1)2.4.2^5 = 3072$
Metrics	$2.2.4.2^5 = 512$	$2.4.2^5 = 256$
Accumulate metric	0	512
CIR update	$2.2.5.2.4.2^5 = 5120$	$2(5+1)2.4.2^5 = 3072$
Total	8192	6912

Table D-2 Example of number of complex calculations.

The number of multiplies dominated and since digital signal processing chips often offer multiply and accumulate function in one cycle 8192 could be used to find the processing power required. Using the PN chip rate from Section 2.1.2, the sampling rate would be 1.2288 Ms/s and the minimum number of cycles per second required would be $8192 \times 1.2288 = 10$ Gs/s. Texas Instruments offer the C64x chip 16 bit fixed point with 4.8 Gs/s. Since the structure was applicable to parallel processing it could have been implemented as an array of processing chips. Using the Xilinx Virtex-II Pro 1000 Gs/s were advertised! So the DSA would be pushing the state of the art.

E. Eye diagram

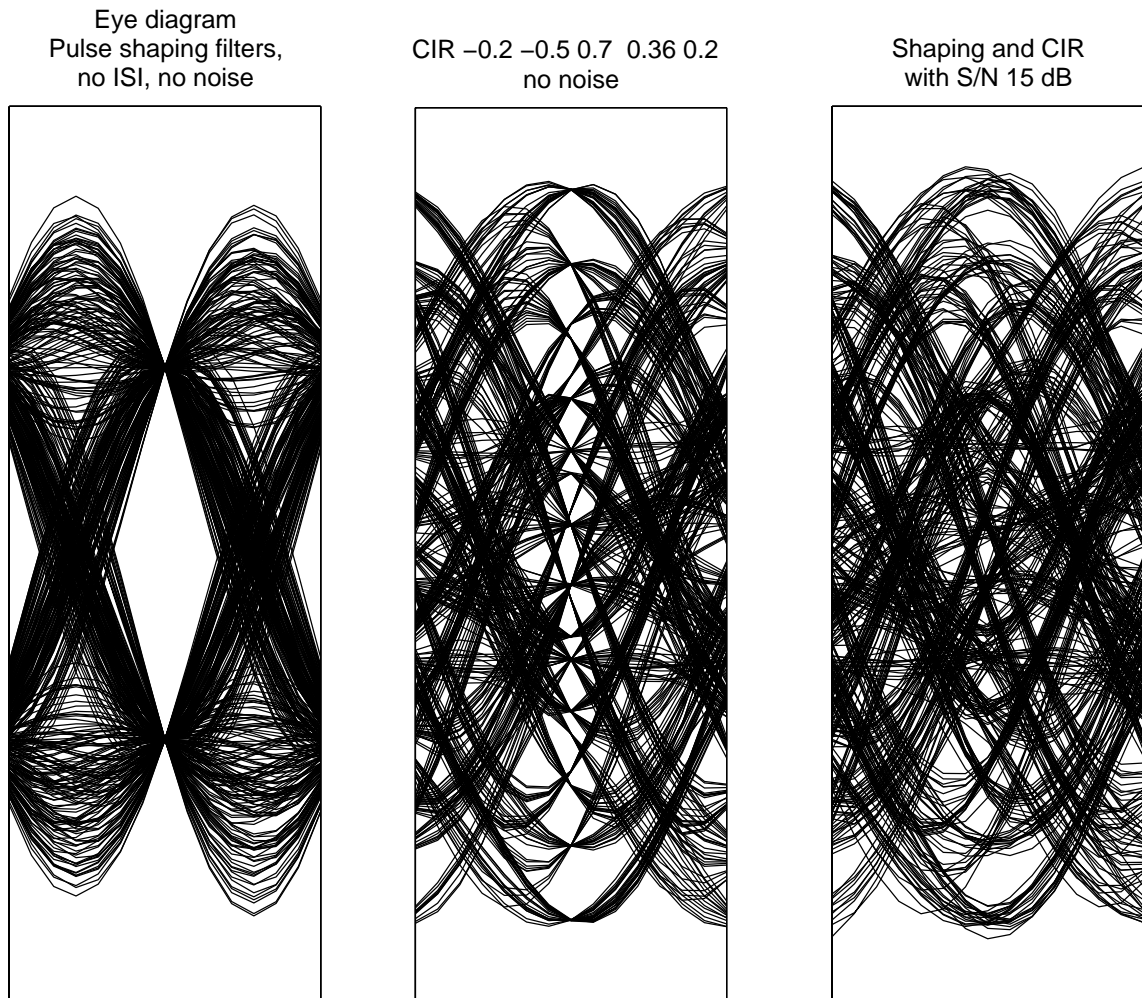


Figure E.1 Eye diagram for CIR2, 15 dB S/N ratio and 25 % excess bandwidth.

The diagrams were made by sampling eight times per symbol and taking 500 trials of the outputs of the three situations; first on the left the transmit and receive filters alone cascaded, second the transmit filter then CIR and then receive filter, and third on the right the transmit, CIR and receive filters with noise added. The resulting waveforms from all the trials were superimposed to form the diagrams. These assumed that the display was triggered with the exact symbol timing.

F. Zeros of the CIRs used

Zeros of CIR1 $-0.2, -0.5, 0.7, 0.36, 0.2$
 CIR2 $0.23, 0.47, 0.69, 0.47, 0.23$
 CIR3 $1.56+0.11i, -0.4-0.34i, -0.04-0.22i, -0.00+0.16i, -0.06-0.15i$
 and CIR4 $1, 1, 0, 0, 0, 0, 0.7$

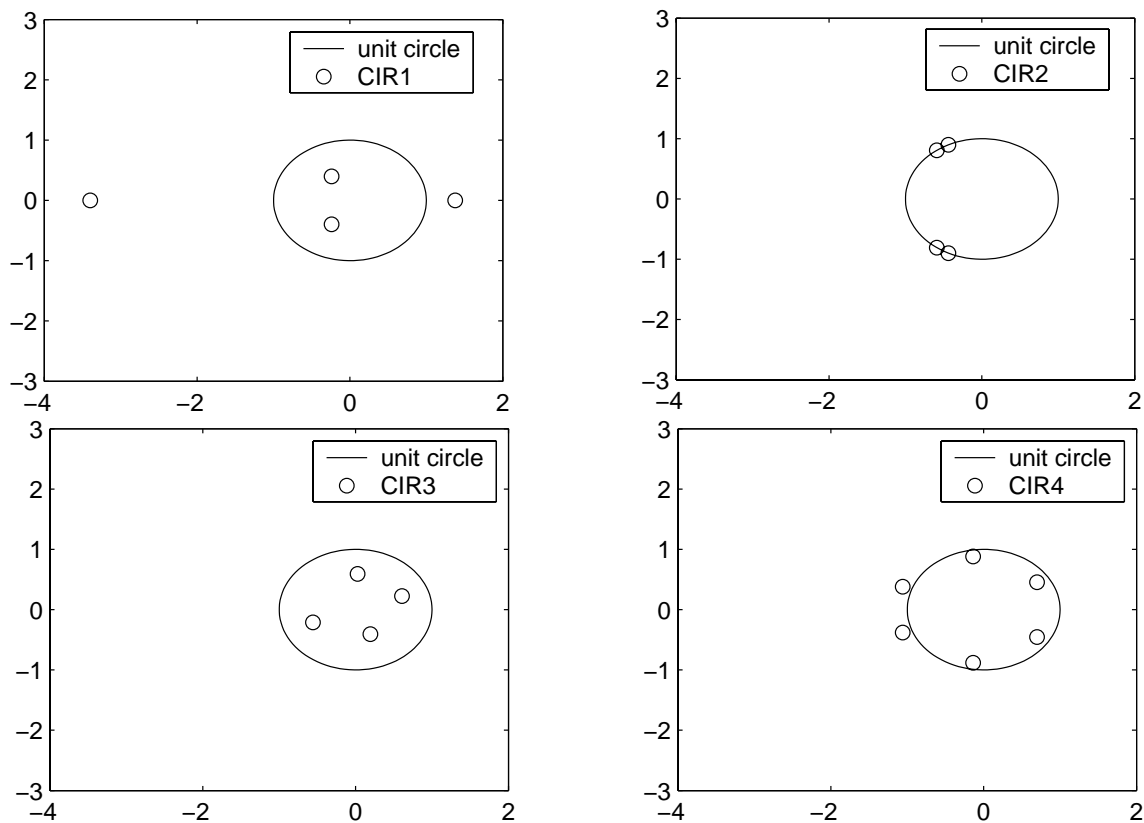


Figure F.1 Zeros of CIRs used showing which have non-minimum phase.

The values plotted are the complex roots of the CIRs, since the paths were assumed to be a FIR type of filter, the roots are the zeros of the transfer function.

G. Learning CIRs for multiple users

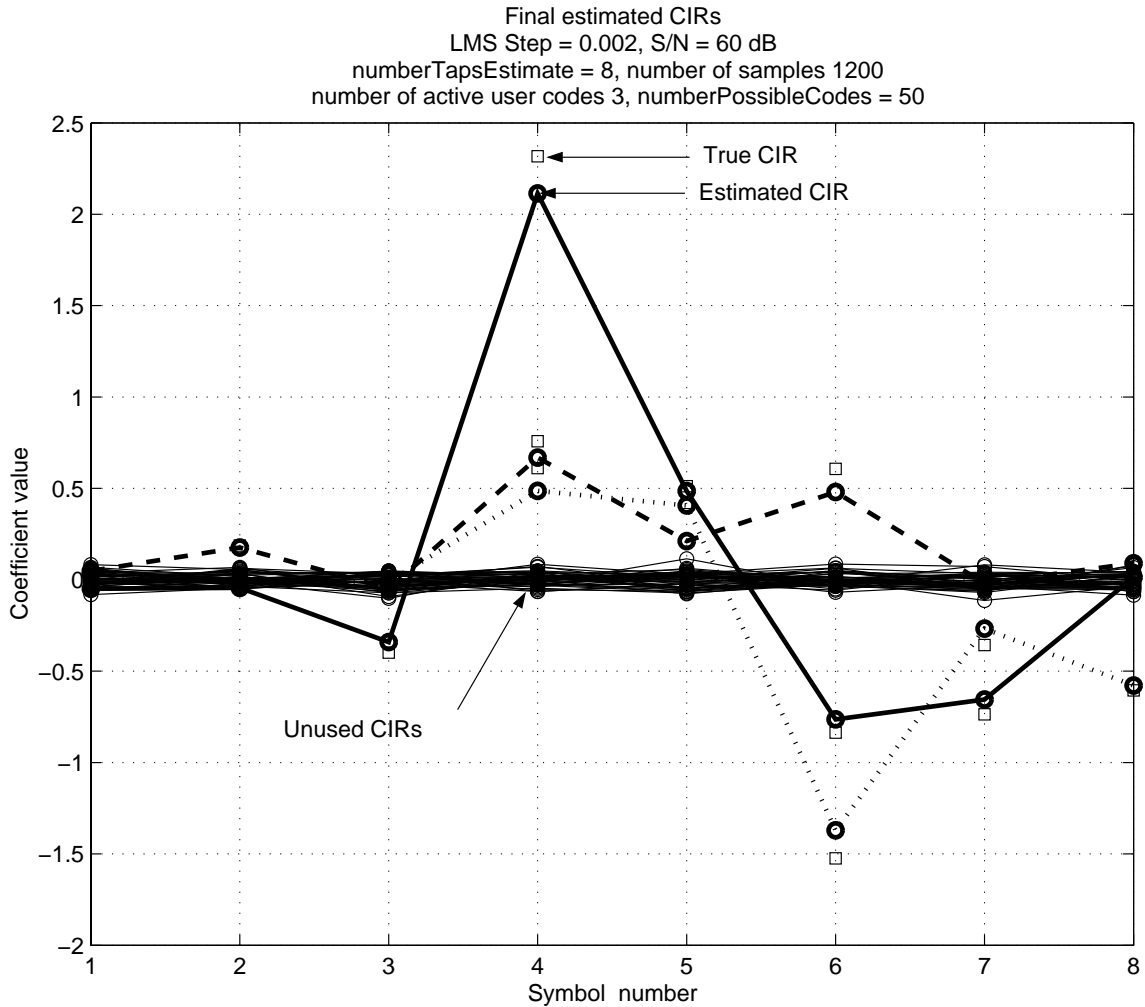


Figure G.1 Resulting CIR estimates for 3 active user codes and 47 unused codes.

The CIRs for multiple users could be extracted by making a new definition of the error and CIR update. Separate errors for each user would be required to do the MLSE and one way may be to separate the CIRs as illustrated. Here the error has to be taken globally rather than in a state by state situation,

$$error = \sum_{u=1}^U \sum_{k=1}^O CIR_{u,k} d_{u,k}, \quad (G.1)$$

where U was the number of possible chip sequences. The LMS update step needed to be optimized taking this into account and converged significantly slower. Since the error was not assigned to individual CIRs during this extraction to run the MLSE on each user the development was required of another stage to remove the contributions to each CIR from all the others, which should not be too difficult. The trellises would be made up of each possible chip sequence at all possible delays.